Chemical Science

ROYAL SOCIETY OF CHEMISTRY

EDGE ARTICLE

View Article Online
View Journal | View Issue

Check for updates

Cite this: *Chem. Sci.*, 2021, **12**, 253

All publication charges for this article have been paid for by the Royal Society of Chemistry

Reappraising Schmidpeter's bis(iminophosphoranyl)phosphides: coordination to transition metals and bonding analysis†

Adrien T. Normand, * E. Daiann Sosa Carrizo, * Corentin Magnoux,‡ Esteban Lobato, Hélène Cattey, Philippe Richard, Stéphane Brandès, Charles H. Devillers, Anthony Romieu, Pierre Le Gendre and Paul Fleurat-Lessard *

Received 28th August 2020
Accepted 25th October 2020

DOI: 10.1039/d0sc04736h

rsc.li/chemical-science

The synthesis and characterization of a range of bis(iminophosphoranyl)phosphide (**BIPP**) group 4 and coinage metals complexes is reported. **BIPP** ligands bind group 4 metals in a pseudo *fac*-fashion, and the central phosphorus atom enables the formation of d^0–d^{10} heterobimetallic complexes. Various DFT computational tools (including AIM, ELF and NCI) show that the phosphorus–metal interaction is either electrostatic (Ti) or dative (Au, Cu). A bridged homobimetallic Cu–Cu complex was also prepared and its spectroscopic properties were investigated. The theoretical analysis of the P–P bond in **BIPP** complexes reveals that (i) **BIPP** are closely related to ambiphilic triphosphenium (**TP**) cations; (ii) the P–P bonds are normal covalent (*i.e.* not dative) in both **BIPP** and **TP**.

Introduction

Geminal dianions stabilized by main group elements have been a topic of interest in main group and coordination chemistry since the 1970s.[1–5] Our understanding of chemical bonding has evolved significantly as a result of numerous insightful studies focused on these species. For instance, double ylides (also known as carbodiphosphoranes, **CDP**) have been instrumental in validating the notion of dative bonding between non-metallic main group elements.[6–11] Thus, **CDP** may be viewed as phosphine complexes of C(0), *i.e.* the C–P bonds are dative covalent.[5,6] The arrow formalism (Scheme 1) is often used to highlight the "metal-like" character of the central carbon atom.

The nature of the C–P bond in these compounds has been rather controversial,[12–16] partly because evidence of C–P bond cleavage in **CDP** and related compounds is scarce:[17] indeed, dative covalent bonds are generally perceived as weak, compared to normal covalent bonds.[14,18] However, the defining feature of dative covalent bonds is their preference for heterolytic bond cleavage in the gas phase (or inert solvents),[18–24] which does not equate with bond weakness.

Isolobal replacement of the central carbon atom in **CDP** by phosphorus yields triphosphenium cations (**TP**, Scheme 1).[25–28] In this case, the dative nature of the P–P bonds seems to be corroborated by the reactivity of **TP**, which readily undergo heterolytic P–P bond cleavage in solution ("ligand exchange", Scheme 2).[29–39] In other words, the arrow formalism acts as a compelling heuristic device to explain the *reactivity* of **TP**. Whether it also relates to the *bonding situation* depends on one's

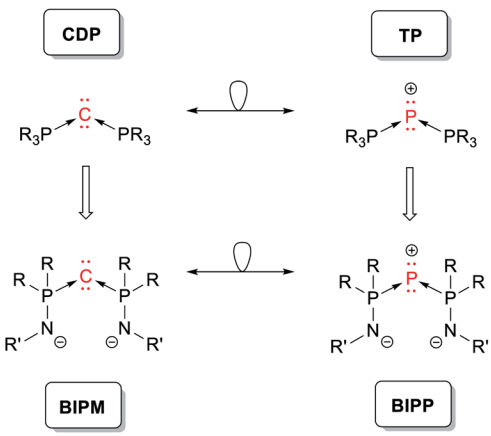

Scheme 1 Selected examples of geminal dianions (**CDP**, **BIPM**) and their phosphorus analogues (**TP**, **BIPP**), all depicted using the arrow formalism.

Institut de Chimie Moléculaire de l'Université de Bourgogne (ICMUB), UMR 6302, CNRS, Université de Bourgogne, 9, Avenue Alain Savary, 21000 Dijon, France. E-mail: adrien.normand@u-bourgogne.fr; eric-daiann.sosa-carrizo@u-bourgogne.fr; paul.fleurat-lessard@u-bourgogne.fr

† Electronic supplementary information (ESI) available: Compounds **2b′**, **3a**, **3b**, **4a**, **5a**, **5b**, **6a**, **6a-Py**, **6b**, **7b**, **8b**, **9b**; detailed procedure for the preparation of P_4; spectra of new compounds. CCDC 1985134–1985146. For ESI and crystallographic data in CIF or other electronic format see DOI: 10.1039/d0sc04736h

‡ Current address: School of Chemistry, The University of Manchester, Oxford Road, Manchester M13 9PL, UK.

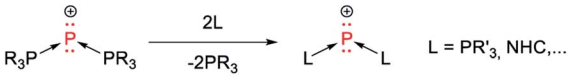

Scheme 2 "Ligand exchange" in triphosphenium cations (TP).

understanding of the arrow formalism. Some authors, who follow Haaland's analysis and use the arrow formalism to depict metal–ligand bonds or main group donor–acceptor adducts (*e.g.* $H_3N \rightarrow BH_3$),[18] might conclude that P–P bonds in **TP** and related compounds are dative covalent (according to IUPAC).[40] This would seem natural, given the reactivity of these compounds in solution. Other authors, who stick to Sidgwick's definition of the "coordinate link"[19] and use arrows in a broader context (*e.g.* to "fix the octet"[24] in compounds such as amine oxides, H_2SO_4, or XeO), will not conclude anything at all.§ Nevertheless, it remains that the bonding situation in **TP** has yet to be addressed with *ad hoc* theoretical tools.[41]

Replacing the phosphine "ligands" in **CDP** by phosphinoamides yields bis(iminophosphoranyl)methanediides (**BIPM**), which act as versatile ligands for a staggeringly broad range of metals.[1–5,42–44] Along with related compounds, **BIPM** have helped challenge the widespread assumption that bonding in lanthanide and actinide complexes is essentially ionic, and that they are not conducive to metal–carbon double bonds.[45–57] It was suggested that **BIPM** may also be viewed as C(0) complexes (Scheme 3, left),[3] but the general agreement is that the P–C bonds are normal covalent.[5,58] Thus most authors in the field feel more comfortable with the alternating dipolar representation (Scheme 3, center)—although those who perpetuate Sidgwick's intellectual heritage might argue that both representations are strictly equivalent. Note that for graphical convenience, the side arms are generally represented with a P=N double bond (Scheme 3, right). This is of course chemically "wrong", but much more legible than the charge-laden (and octet rule-abiding) resonance form.

Very little is known about the phosphorus analogues of **BIPM**, *i.e.* bis(iminophosphoranyl)phosphides (**BIPP**): a single derivative was reported in 1985 by Schmidpeter, and characterized by ^{31}P NMR spectroscopy only.[59,60] We surmised that these compounds could offer a unique opportunity to introduce a phosphide ligand in the coordination sphere of group 4 metals (Scheme 4), an area which we have been investigating for some time.[61–64] We also became interested in comparing their properties to those of **TP**, with a particular focus on the nature—normal or dative covalent—of P–P bonds, and the possibility to prepare early-late heterobimetallic complexes (by coordination

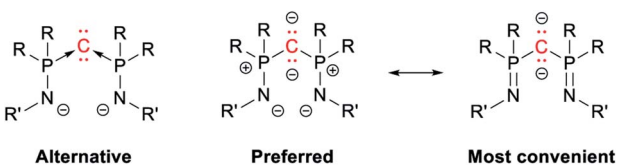

Scheme 3

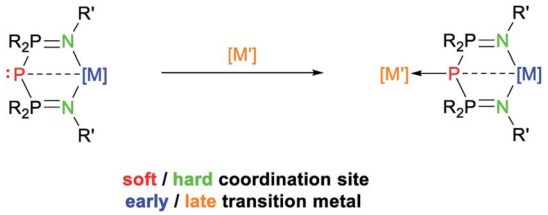

Scheme 4 Targeted early (left) and early/late (right) metal complexes of BIPP.

of a late transition metal to the central phosphorus atom).[32,34–37,65–68]

Results and discussion

Ligands synthesis

Schmidpeter described the synthesis of **BIPP** anions starting either from white phosphorus (P_4) or from [K(18-crown-6)][$\mathbf{P(CN)_2}$].[59,60] We found it more convenient and cost-effective to use P_4 since the synthesis of the $\mathbf{P(CN)_2}^-$ anion also starts from P_4.[69] The downside of using P_4—aside from its well-documented toxicity and pyrophoric character—is that it is not commercially available in Europe anymore, and therefore has to be prepared following a procedure developed by Baker in the XIXth century. This consists in the thermal allotropic conversion of red phosphorus into white phosphorus.[70] More recently, Arnold, Hsu and Tsai adapted this procedure to modern day Schlenk-line techniques.[71] We independently developed a safer variation of Baker's allotropic conversion, using a custom-made silica glass Schlenk flask for improved heat resistance (see the ESI† for details).

Thus, heating lithium phosphinoamides **1** with an excess of P_4 (2 to 2.4 eq.) at 100 °C in 1,4-dioxane afforded **BIPP**–Li proligands **2** in moderate to good yields (Scheme 5). Replacing 1,4-dioxane by THF in the case of phosphinoamide **1b** afforded compound **2b′** in lower yield, but enabled to grow single crystals for X-ray diffraction analysis (*vide infra*). Whilst not completely optimal, this procedure easily affords multigram quantities of **2**. Proligands **2** were characterized by multinuclear NMR spectroscopy, IR and UV-Vis spectroscopies, elemental analysis and, in the case of **2b′**, XRD analysis.

All other compounds in this study were characterized similarly. Relevant $^{31}P\{^1H\}$ NMR parameters, such as the chemical shifts of lateral (δP_L) and central (δP_C) P atoms, along with the $^1J_{PP}$ coupling constants values, are gathered in Table 1.

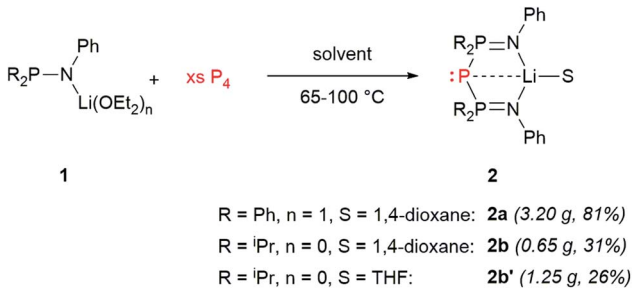

Scheme 5 Synthesis of BIPP–Li proligands.

Table 1 $^{31}P\{^{1}H\}$ NMR parameters of diamagnetic **BIPP** complexes and related compounds[a]

Compound	Metal	δP_L (ppm)	δP_C (ppm)	$^{1}J_{PP}$ (Hz)
2a	Li	31.8	−118.7	411
2b	Li	62.2	−201.6	462
2b′	Li	61.0	−190.8	450
4a	Ti	32.5	−212.9	381
5a	Zr	27.2	−210.2	351
5b	Zr	56.9	−223.0	384
6a	Ti	37.4	−179.2	416
6a-Py	Ti	34.5	−189.3	390
6b	Ti	67.7	−241.0	474
7b	Ti/Au	73.7	−160.4	347
8b	Ti/Cu	70.2	−212.8	414
9b	Cu	59.2	−146.2	349
A[b]	—	34.1	−220.9	414
B[b]	—/Au	31.3	−108.7	314

[a] Spectra recorded in CD_2Cl_2 at 298 K except for Li complexes (THF-d_8), **2b** (293 K), **4a** (260 K), **5a** (291 K), **6a**/**6a′** (292 K), **8b** (290 K). [b] See ref. 34.

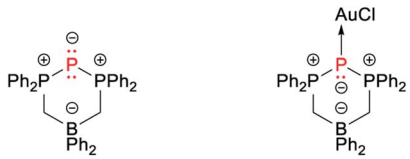

A B

Chart 1 Selected compounds from the literature.

The $^{31}P\{^{1}H\}$ NMR spectrum of **BIPP** complexes corresponds to an A_2X spin system: the lateral P atoms resonate as a doublet in the positive region of the spectrum, whilst the central P atom resonates as a strongly shielded triplet. The δP_C value is quite sensitive, even to remote changes in the environment around the central P atom. Thus, whilst the δP_L value of **2b** and **2b′** are quite close ($\Delta\delta P_L = 1.2$ ppm), the difference between δP_C values is much larger ($\Delta\delta P_C = 10.8$ ppm), especially considering that both compounds only differ by the solvent molecule coordinated to Li (1,4-dioxane *vs.* THF). The values reported in Table 1 for **BIPP** compounds are comparable to those reported for compounds **A** and **B** (Chart 1). The dicoordinate¶ central phosphorus of **A** shows typical "ligand exchange" reactivity in the presence of strongly donating phosphines.[34]

The XRD structure of **2b′** is shown in Fig. 1. The unit cell was found to contain one molecule of **2b′** with disordered ^{i}Pr groups (borne by P1) and one disordered THF molecule. Relevant metric parameters for **BIPP** complexes and related compounds **A** and **B** are given in Table 2.

The main features of the solid-state structure of **2b′** are (i) its low symmetry, noticeable in the orientation of the Ph rings *away* and *above* the LiNPPPN ring; (ii) the large P2–Li distance (3.909(6) Å), far superior to the sum of covalent radii for Li and P (2.35 ± 0.10 Å),[72] and close to the sum of van der Waals radii (4.02 Å);[73] (iii) the slightly obtuse P1–P2–P3 angle (102.64(4)°). The latter feature is shared between all compounds reported in Table 2. Indeed, the angle between the central P atom and its substituents ranges from 94.59(9)° in **B** to 109.84(3)° in **9b**. Likewise, the P–P bond distances in **2b′** (2.143 Å on average) fall within the rather narrow range of values reported in Table 2 (from 2.1293(6) Å for **6b-2** to 2.2332(6) for **9b**).

BIPP coordination to group 4 metals

With ligands **2** in our hands, we turned to the synthesis of Ti and Zr complexes. Reaction of **2a** and **2b** with $[TiCl_3(THF)_3]$ in THF gave **3a** and **3b**, respectively, after workup (Scheme 6).

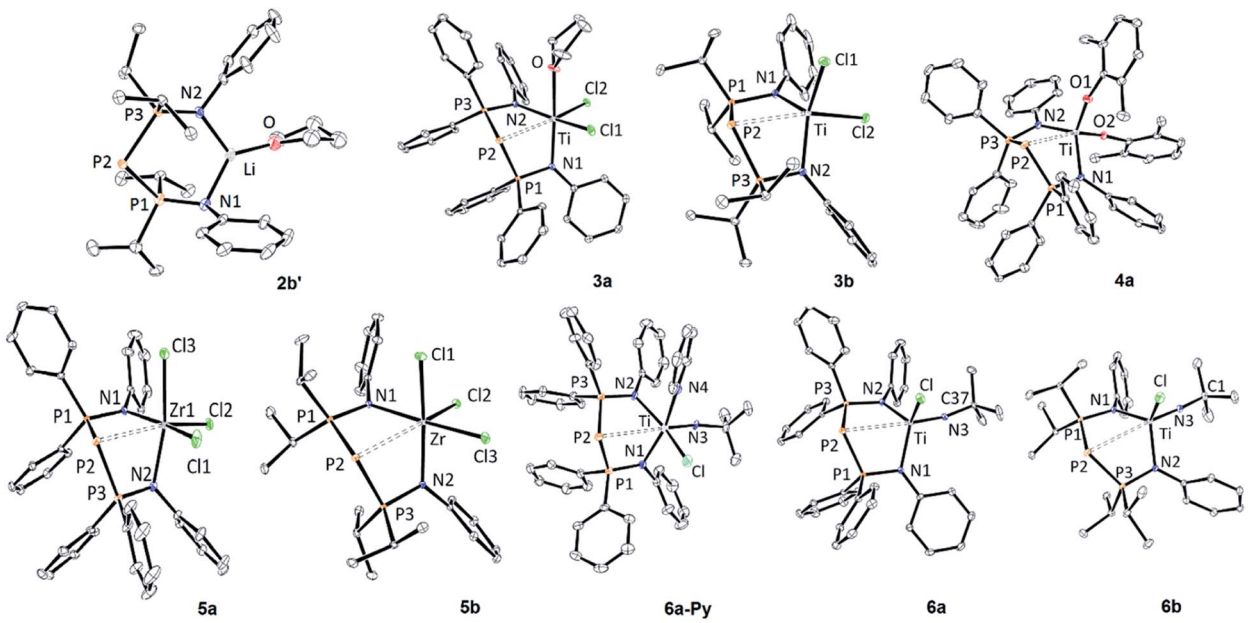

Fig. 1 ORTEP depiction of the X-ray structures of monometallic **BIPP** complexes (thermal ellipsoids drawn at the 30% probability level, solvent molecules, BPh_4^- anion (for **4a**), hydrogen and disordered atoms are not shown for clarity). For **5a** and **6b** only one independent molecule is shown (**5a-1** and **6b-1**). See Table 2 for metric parameters. See the ESI† for additional bond distance and angles.

Table 2 Selected bond distances (Å) and angles (°) for complexes **2b′–9b** and relevant compounds from the literature

Compound	Metal	P2–M[a]	P1–P2	P2–P3	N1–P1	N2–P3	N1–M	N2–M	P1–P2–P3	N1–M–N2
2b′	Li	3.909(6)	2.1359(11)	2.1509(10)	1.619(2)	1.614(2)	1.962(6)	1.936(6)	102.64(4)	111.5(2)
3a	Ti	*2.7712(6)*	2.1558(7)	2.1333(6)	1.6345(14)	1.6278(14)	2.1024(14)	2.1611(14)	98.72(2)	97.77(5)
3b	Ti	2.7832(6)	2.1626(7)	2.1424(6)	1.6400(14)	1.6374(14)	2.0116(13)	2.0501(14)	108.45(2)	110.02(6)
4a	Ti	2.8125(13)	2.1415(14)	2.1460(15)	1.640(3)	1.646(3)	2.023(3)	2.014(3)	102.25(6)	114.19(13)
5a-1[b]	Zr	2.8896(5)	2.1566(6)	2.1621(6)	1.6236(14)	1.6337(15)	2.1960(15)	2.1868(15)	99.19(2)	90.37(5)
5a-2[b]	Zr	2.8961(6)	2.1649(7)	2.1499(7)	1.6336(15)	1.6299(15)	2.1960(15)	2.1893(15)	100.81(3)	88.63(6)
5b	Zr	*2.8327(5)*	2.1502(6)	2.1553(6)	1.6381(13)	1.6371(13	2.2168(13)	2.1713(13)	106.11(2)	99.22(5)
6a-Py	Ti	3.078(2)	2.138(2)	2.144(2)	1.615(5)	1.621(5)	2.112(5)	2.131(5)	99.50(9)	93.12(19)
6a	Ti	3.0308(7)	2.1434(8)	2.1388(8)	1.6464(19)	1.6379(19)	2.0758(19)	2.0256(19)	103.57(3)	107.72(7)
6b-1[b]	Ti	3.1049(6)	2.1404(5)	2.1531(5)	1.6422(13)	1.6409(13)	2.0372(13)	2.0257(13)	108.98(2)	108.19(5)
6b-2[b]	Ti	3.0706(5)	2.1293(6)	2.1494(6)	1.6453(13)	1.6496(13)	2.0470(13)	2.0391(13)	106.74(2)	108.87(5)
7b	Ti/Au	2.9823(12)/2.2240(10)	2.1884(9)	2.1884(9)	1.637(2)	1.637(2)	2.037(2)	2.037(2)	106.31(5)	103.38(10)
8b	Ti/Cu	3.1159(10)/2.1948(9)	2.1682(11)	2.1676(12)	1.632(3)	1.637(3)	2.029(3)	2.038(3)	109.39(5)	104.90(11)
9b	Cu	*2.1798(5)*	2.1631(6)	2.2332(6)	1.6296(15)	1.5814(16)	1.8989(15)	—	109.84(3)	—
A[c]	—	—	2.1371(9)	2.1328(9)	—	—	—	—	95.70(3)	—
B[c]	—/Au	*2.2512(17)*	2.200(2)	2.174(2)	—	—	—	—	94.59(9)	—
C[b,d]	Ti	2.599(2)[e]	—	—	1.636(2)	1.630(2)	2.052(2)	2.040(2)	—	108.53(7)

[a] Italicized values indicate bond distance < sum of covalent radii (Alvarez, ref. 72). [b] Two independent molecules in the unit cell. [c] See ref. 34. [d] See ref. 78. [e] C–M distance.

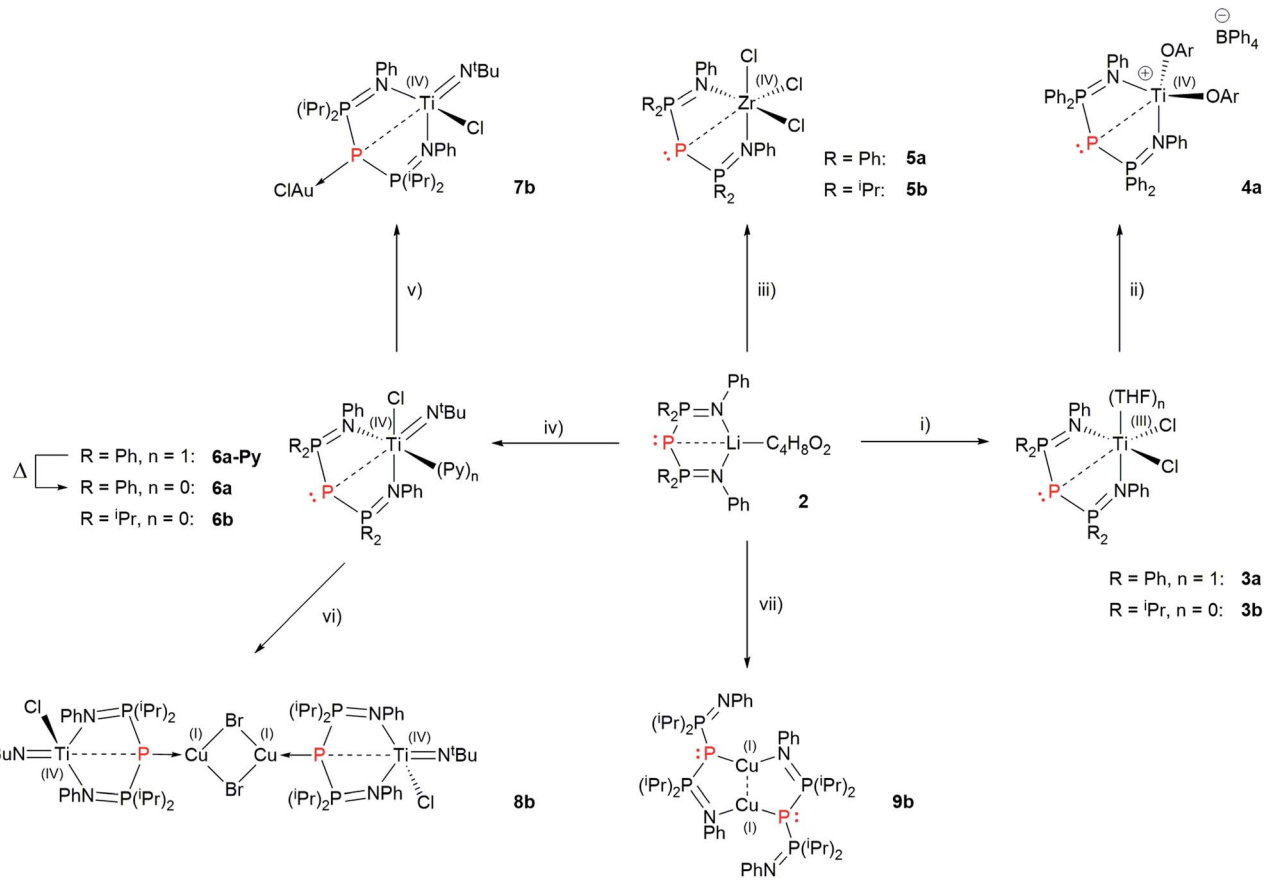

Scheme 6 Synthesis of group 4 and coinage metal complexes of **BIPP**. Reagents and conditions: (i) 1 eq. $[TiCl_3(THF)_3]$, THF; (ii) 1 eq. $[Cp_2Fe][BPh_4]$, 2 eq. ArONa (OAr = 2,6-dimethylphenolato); (iii) 1 eq. $ZrCl_4$, toluene; (iv) 1 eq. $[TiCl_2(N^tBu)(Py)_3]$, toluene; (v) 1 eq. [Au(THT)Cl], CH_2Cl_2; (vi) 1 eq. CuBr, CH_2Cl_2; (vii) 1 eq. CuBr, toluene. All reactions were conducted at room temperature (THT = tetrahydrothiophene).

The room temperature EPR spectra of **3a** and **3b** in THF are very similar and characterized by a single absorption line (**3a**: $g = 1.9524$; **3b**: $g = 1.9520$) with hyperfine coupling to Ti (**3a**, **3b**: $A^{47/79}$ Ti = 15.7 10^{-4} cm^{-1}). Interestingly, no super-hyperfine coupling to P or N was observed.[74]

The X-ray structures of **3a** and **3b** are shown in Fig. 1. In contrast with **2b′**, these compounds display much shorter P–M distances, with values reaching the upper limit of the sum of covalent radii (Table 2). Remarkably, complex **3a** contains one coordinated molecule of THF, whilst **3b** is solvent-free (both compounds crystallized from THF solutions). Consequently, **3a** displays a distorted octahedral geometry along three axes (Cl1–Ti–N2; Cl2–Ti–P2; N1–Ti–O), whilst **3b** is best described as a distorted trigonal bipyramid built along the Cl2–Ti–P2 unique axis. The extra ligand in **3a** leads to elongated average Ti–N distances compared to **3b**, as well as a narrower N1–Ti–N2 angle. On the other hand, intra-ligand distances, *e.g.* average P–P and P–N bond distances, are quite similar in both complexes (**3a**: P–P = 2.145 Å, P–N = 1.631 Å; **3b**: P–P = 2.155 Å, P–N = 1.639 Å).

Together with Erker, we have shown that cationic d^0 group 4 metallocene complexes containing a phosphorus ligand (phosphide or phosphine) display frustrated Lewis pair (FLP) behaviour;[61–64,75] therefore we were keen to explore the possibility of generating post-metallocene Ti(IV) cations from complexes **3**. Oxidation of **3a** by $[Cp_2Fe][BPh_4]$ in THF, followed by salt metathesis with sodium 2,6-dimethylphenolate etherate yielded complex **4a** in 66% yield after workup (Scheme 6). In the case of **3b**, the same procedure yielded an intractable mixture of compounds.

The ^{1}H NMR spectrum of **4a** at 300 K reveals the fluxionality of the PPh and OAr groups (Fig. S30†). Cooling to 260 K enabled to partly freeze the structure, although free rotation of each OAr group around O–C_{Ar} bonds was still observed. Compared to ligand **2a**, the central P atom in **4a** resonates at much higher field in the $^{31}P\{^1H\}$ spectrum (−212.9 *vs.* −118.7 ppm, see Table 1); however, in light of the δP_C value for other **BIPP^{Ph}** compounds, it appears that **2a** is the outlier.

Considering the sensitivity of the P2–M bond distance to crystal packing forces (*vide infra*), the P2–Ti bond distance in **4a** is also very similar to that in **3a** and **3b** (Δd < 0.05 Å). At 2.8125(13) Å it is distinctly superior to the sum of covalent radii for Ti and P, hinting at the possibility of FLP reactivity.[76] However, the reaction mixture of **4a** and ferrocene carboxaldehyde (FcCHO) in CD_2Cl_2 remained unchanged; we had previously observed that FcCHO is one of the most reactive substrates against Ti/P FLPs,[64,75] therefore we did not investigate the FLP behaviour of **4a** any further. Instead, we turned our attention to Zr complexes, which generally display enhanced FLP reactivity compared to Ti.[61,64]

We synthesized Zr complexes **5** by salt metathesis between $ZrCl_4$ and ligands **2**. After workup, complexes **5a** and **5b** were obtained in 67% and 71% yield respectively (Scheme 5). The $^{31}P\{^1H\}$ NMR spectra of **5a** and **5b** both display a strongly shielded signal for the central P atom (−210.2 and −223.0 ppm, Table 1). Interestingly, these values are quite close ($\Delta\delta P_C$ = 12.8 ppm), whereas the central P atoms in ligands **2a** and **2b** resonate at vastly different frequencies ($\Delta\delta P_C$ = 82.9 ppm).

The X-ray structures of **5a** and **5b** are shown in Fig. 1. Two independent molecules of **5a** are present in the unit cell, but their metric parameters are very similar (Table 2). The P2–Zr bond distance is very similar in **5a-1**, **5a-2** and **5-b**, just within the sum of covalent radii for Zr and P. Both **5a** and **5b** display a distorted octahedral geometry along Cl1–Zr–N2, Cl2–Zr–P2 and Cl3–Zr–N1 axes. Due to the pseudo octahedral geometry, the N1–Zr–N2 angles in both compounds (*e.g.* **5a-2**: 88.63(6)°; **5b**: 99.22(5)°) are rather small compared to other less crowded complexes (*e.g.* **6a**: 107.72(7)°, **3b**: 110.02(6)°). As mentioned above, the larger variations observed for the **BIPP^{Ph}** ligand are a probable consequence of the flexibility conferred by the PPh_2 groups.

Interestingly, the Cl ligands in octahedral **BIPP** complexes experience a clear structural *trans* effect (STE) from the iminophosphorane side arms (see Table S13†).[77] This is in line with the non-covalent nature of the interaction between P2 and M (*vide infra*).

Complexes **5** gave intractable mixtures of compounds upon reaction with sodium 2,6-dimethylphenolate, therefore we were unable to synthesize the Zr analogues of **4a**. In an ultimate attempt to investigate the FLP behaviour of Zr complexes, we reacted **5b** with FcCHO in C_6D_5Br, but we only observed a slight broadening of the central phosphorus atom signal at room temperature, and product decomposition at 60 °C.

The "boat" conformation of complexes **3–5** is reminiscent of the coordination behavior of bis(iminophosphoranyl)methanide ligands (**BIPMH**), which are the conjugate acids of **BIPM**.[2] We have previously reported the only known examples of Ti–**BIPMH** complexes.[78] Such compounds may be synthesized by salt metathesis between **BIPMH** anions and $[TiCl_2(N^tBu)(Py)_3]$ (Mountford's complex). Applying this procedure to ligands **2** gave complexes **6a-Py** and **6b** in 50% and 81% yield, respectively, after workup (Scheme 6). The pyridine-free complex **6a** was obtained in 74% yield by heating a toluene solution of **6a-Py** to reflux.

The ^{1}H NMR spectrum of **6a-Py** displays characteristic signals corresponding to the pyridine ligand (multiplets at 9.17, 7.68 and 7.32–7.19 ppm). Pyridine loss induces noticeable changes in the $^{31}P\{^1H\}$ spectrum of **6a** compared to **6a-Py**: the lateral and central P atoms resonate at higher field ($\Delta\delta P_L$ = −2.9 ppm; $\Delta\delta P_L$ = −10.1 ppm), and the $^1J_{PP}$ coupling constant is slightly weaker (Δ^1J_{PP} = −26 Hz).

Fig. 1 shows the X-ray structure of **6a** and **6a-Py**. For **6a-Py**, the analysis confirmed that the pyridine molecule is bound to Ti, and occupies one of the axial positions of the distorted octahedron. Interestingly, complex **6a** crystallizes with one disordered molecule of toluene, despite the fact that the crystals were obtained by diffusion of pentane into a CH_2Cl_2 solution of **6a** (1 eq. of toluene was also observed by NMR spectroscopy in microcrystalline samples of **6a**). The P2–Ti distances in both complexes are considerably longer than the sum of covalent radii, but other distances and angles are unremarkable within the series of compounds reported in Table 2.

The distorted trigonal planar geometry of **6a** is very similar to that of its **BIPMH** analogue (**C**), as shown by the comparison of metric parameters in Table 2 and the superimposed structures (shown in Fig. S127†). The main difference between **6a** and **C** is the longer E–Ti (E = P, C) bond distance between the metal and the central, negatively charged atom, due to the larger size of phosphorus.[72,73] These observations highlight the structural analogy between **BIPP** and **BIPMH** ligands.

Fig. 1 shows the crystal structure of one of the two independent molecules of **6b**. Again, a distorted planar geometry is observed for **6b-1** and **6b-2** (not shown). The P2–Ti distance is clearly superior to the sum of covalent radii for P and Ti in both cases, but it is noticeably shorter in **6b-1** ($\Delta d = -0.0343(8)$ Å). As suggested by the superimposed structures of **6b-1** and **6b-2** (shown in Fig. S128†), this difference could originate from conformational changes, *i.e.* different orientations of the ^{i}Pr and Ph groups.

BIPP coordination to group 10 metals

The long P2–Ti distance in **6a** and **6b** suggests that the interaction between both atoms is non-covalent (*vide infra*). A logical consequence is that it should be possible to coordinate one or two late transition metals to the central P atom, similarly to **TP** cations.

Reaction of **6a** with [AuCl(THT)] (THT = tetrahydrothiophene) in CD_2Cl_2 yielded a complex mixture. However, clean formation of a new compound was observed in the case of **6b**. When the reaction was repeated on preparative scale, complex **7b** was isolated in 48% yield. Similarly, reaction of **6b** with CuBr yielded complex **8b** in 78% isolated yield (Scheme 6).

Coordination of AuCl and CuBr fragments to **6b** has a dramatic impact on the $^{31}P\{^{1}H\}$ NMR spectrum (Table 1). The $^{1}J_{PP}$ coupling constant decreases considerably (**7b**: $\Delta^{1}J_{PP} = -127$ Hz; **8b**: $\Delta^{1}J_{PP} = -60$ Hz), whilst the central phosphorus atom resonates at much lower field (**7b**: $\Delta\delta P_C = 80.6$ ppm; **8b**: $\Delta\delta P_C = 28.2$ ppm). In the case of **8b**, the corresponding signal is very broad, due to the coordination to Cu. Finally, the lateral phosphorus atoms resonate at slightly lower field (**7b**: $\Delta\delta P_L = 6.0$ ppm; **8b**: $\Delta\delta P_L = 2.5$ ppm).

Complex **7b** decomposes quite rapidly in CD_2Cl_2 solutions: decomposition products can already be observed in freshly prepared samples. A probable explanation for this behaviour is that the electron-donating properties of **6b** are insufficient. This is also consistent with the impossibility to stabilize AuCl with **6a**. By contrast, **8b** does not show signs of decomposition in solution. Since the central phosphorus atom in complexes **6** possesses two free lone pairs (*vide infra*), we attempted to coordinate two CuBr fragments to **6b**, however we could only observe the formation of **8b**.

Fig. 2 shows the structure of **7b** and **8b**. These are rare examples of structurally characterized examples of d^0/d^{10} heterobimetallic complexes bridged by a phosphorus atom.[79–83] Both complexes show some disorder (the ^{t}Bu group in the case of **7b**, one of the Ph groups in the case of **8b**).

The structural changes observed upon coordination of the coinage metal fragment to **6b** are quite subtle. In the case of gold (**7b**), the P2–Ti distance becomes slightly shorter, although still superior to the sum of covalent radii. The P–P distances become slightly longer, which could be due to back-bonding between the electron-rich d^{10} metal and the **BIPP** ligand (see the AIM results in the ESI†). In the case of copper (**8b**), the P2–Ti and P–P bond distances become slightly elongated compared to **6b**. In both cases, the central P atom adopts an AX_3E geometry (**7b**: $\sum\alpha(P2) = 327.51(8)°$; **8b**: $\sum\alpha(P2) = 333.31(8)°$). The Au–P2 distance in **7b** is close to those observed in Au–**TP** complex **B** (Table 2), as well as in $[AuCl(PR_3)]$ complexes reported by Schmidbaur. (R = Me: 2.233(3) Å; R = ^{i}Pr: 2.239(2) Å).[84]

No Cu–**TP** complexes have been reported yet, but the Cu–P2 bond distance in **8b** is very close to those observed for dimeric $[Cu(\mu\text{-Br})(PR_3)]_2$ complexes reported by Healy (~2.20 Å).[85]

In light of the above, it appears that the net electron-donating properties of **6b** are close to weakly basic **TP** cations such as **A** (which can only bind one AuCl fragment). We wondered whether the more reactive Li complexes **2** could entail stronger electron donation and/or different coordination modes to coinage metals. Reaction of **2a** with [Au(THT)Cl] and CuBr in C_6D_6 gave a complex mixture and an insoluble solid that could not be analysed by NMR spectroscopy, respectively. Reaction of **2b′** with [Au(THT)Cl] gave a complex mixture.‖ However, reaction of **2b** with CuBr gave a single new product. When the reaction was conducted in toluene instead of C_6D_6, complex **9b** was isolated in 67% yield (Scheme 6).

The ^{1}H and $^{31}P\{^{1}H\}$ NMR spectra of **9b** in CD_2Cl_2 at 298 K belie the solid-state structure depicted in Fig. 2: indeed, only

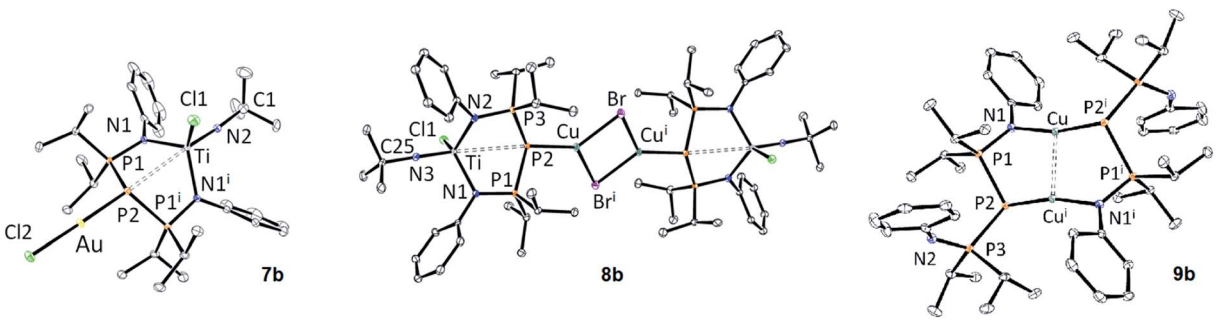

Fig. 2 ORTEP depiction of the X-ray structures of **7b**, **8b** and **9b** (thermal ellipsoids drawn at the 30% probability level, hydrogen atoms, solvent molecules and disorder are not shown for clarity). See Table 2 for metric parameters. See the ESI† for additional bond distance and angles.

one set of signals is observed for the Ph and ^{i}Pr groups in the ^{1}H NMR spectrum. The ^{31}P{^{1}H} NMR spectrum offers an explanation, since the signal of the lateral phosphorus atoms is visibly broad. Upon cooling to 250 K, this signal broadens to the extent that the $^{1}J_{PP}$ coupling constant is not distinguishable anymore (Fig. S104†). A possible explanation for the observed fluxionality of **9b** would be iminophosphorane arm exchange following a dissociative mechanism, or central phosphorus exchange following an associative mechanism (*via* a P-bridged intermediate).

Compared to other **BIPP** complexes reported in this study, **9b** displays remarkable optical spectroscopic features. For instance, the IR spectrum shows a strong absorption at 1335 cm^{-1} in an otherwise empty region of the spectrum (Fig. 3). Analysis of the normal modes for **9b** by DFT revealed that the strong absorption at 1335 cm^{-1} is due to N–C_{Ph} stretching of the free iminophosphorane arm (see multimedia file), which explains why it is not visible in κ^3-N,P,N-coordinated compounds.

Additionally, the UV-Vis spectrum in CH_2Cl_2 shows an intense absorption at 336 nm (ε = 12 000 M^{-1} cm^{-1}). The latter is reminiscent of the behaviour of cationic dimeric complexes [Cu(dcpm)$_2$]$_2$[X$_2$] reported by Che (**D**, Chart 2; dcpm = bis(dicyclohexylphosphine)methane). These complexes also display a strong absorption centred at 307–311 nm ($\varepsilon \approx$ 14 000–17 000 M^{-1} cm^{-1}), which has been ascribed to a metal–metal 3d → 4p transition.[86,87]

Interestingly, the bicyclic structure of **9b** can also be related to those of **D**. Focussing on $\mathbf{D}_{BF4}$, the Cu–Cu distance is close, although slightly shorter in **9b** (2.5759(4) *vs.* 2.691(2) Å). The P2^{i}–Cu distance in **9b** (2.1798(5) Å) is also slightly shorter than the average P–Cu distance in $\mathbf{D}_{BF4}$ (2.22 Å). These spectroscopic and structural similarities prompted us to investigate the luminescence properties of **9b**, since complexes **D** were found to be weakly emissive in solution and in the solid state; however, in our case no fluorescence could be observed in solution (CH_2Cl_2, THF) or in the solid state upon excitation at 336 nm.

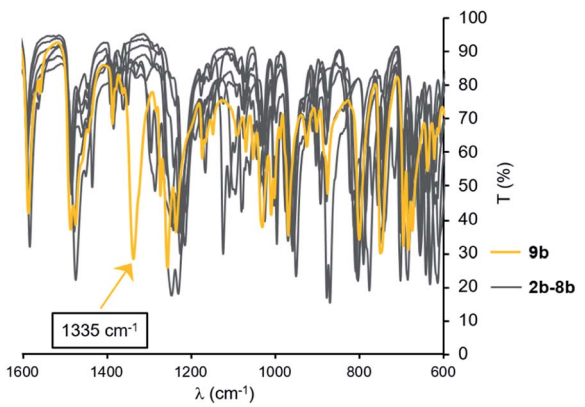

Fig. 3 IR spectra of **BIPP** complexes **2b–9b** (ATR, 1600–600 cm^{-1} range).

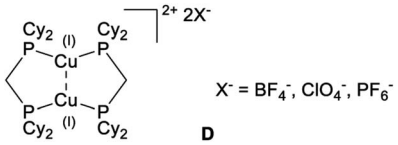

Chart 2 Luminescent Cu(I) complexes resported by Che.

In order to understand the lacklustre photophysical properties of **9b** compared to **D**, we computed their absorption spectra with TD–DFT. The computed absorption wavelengths were found in fair agreement with the experimental one: 359 nm instead of 336 nm for **9b** and 289 nm instead of 310 nm (average) for $\mathbf{D}^{+}$. In both computed complexes, this absorption corresponds to a HOMO to LUMO transition. As postulated by Che,[86,87] this transition has 3d → 4p character. In the case of **9b**, both the HOMO and the LUMO are actually quite developed on the phenyl groups of the phosphorus atoms (Fig. S119†), and hence the contribution of the Cu orbitals in this S_0–S_1 transition is smaller than in the case of $\mathbf{D}^{+}$. This suggests that the phenyl groups in **9b** are probably responsible for quenching the fluorescence, as noted elsewhere.[88] As a corollary, replacing the phenyl groups in **9b** by alkyl groups should restore the fluorescence.

Finally, we conducted voltammetric analyses on **9b** (THF, 0.1 M $NaBPh_4$). Several non-reversible events took place both in oxidation and reduction, which could not be interpreted (see Fig. S105†).

Bonding analysis

The above experimental results raise a number of questions pertaining to the bonding situation in **BIPP** complexes. Bearing in mind the broader context of the nature of bonding in main group compounds, one may thus ask:

(i) How do **BIPP** complexes compare to **TP** cations and related dicoordinate phosphorus compounds?

(ii) Is the arrow formalism relevant to represent the P–P bonding situation in **BIPP** complexes?

(iii) What is the nature of the P–Ti interaction?

In order to address these questions, density functional theory (DFT) calculations were conducted on complexes **6a**/**6b**, **7a**/**7b** and **9b**, along with ambiphilic dicoordinate phosphorus compounds **A** and $\mathbf{P(CN)_2}^{-}$. All compounds were computed in toluene using the Polarizable Continuum Model (PCM). The bonding situation was analysed and/or represented using the following computational tools: molecular orbitals, Electron Localization Function (ELF) analysis,[89–93] Electrostatic Potential Maps (EPM),[94] Bader's Atoms in Molecules (AIM),[95–97] and Non-Covalent Interactions (NCI) plots.[98,99]

The computed bond lengths and angles are in good agreement with the experimental solid state structures. In general, the observed deviations are modest (<3%). Notable exceptions include the P2–M distances in **6a** and **6b**, and the P1–P2–P3 angle in **6a** and **A**, which deviate by up to ±8%.

Molecular orbitals. The frontier molecular orbitals of **6a**, **6b**, **A**, $\mathbf{P(CN)_2}^{-}$ and **9b** are shown in Fig. 4. As expected, in **6a**, **6b**, **A** and $\mathbf{P(CN)_2}^{-}$, the lone pair of the central phosphorus atom (P_2) largely contributes to the HOMO while the LUMO develops on

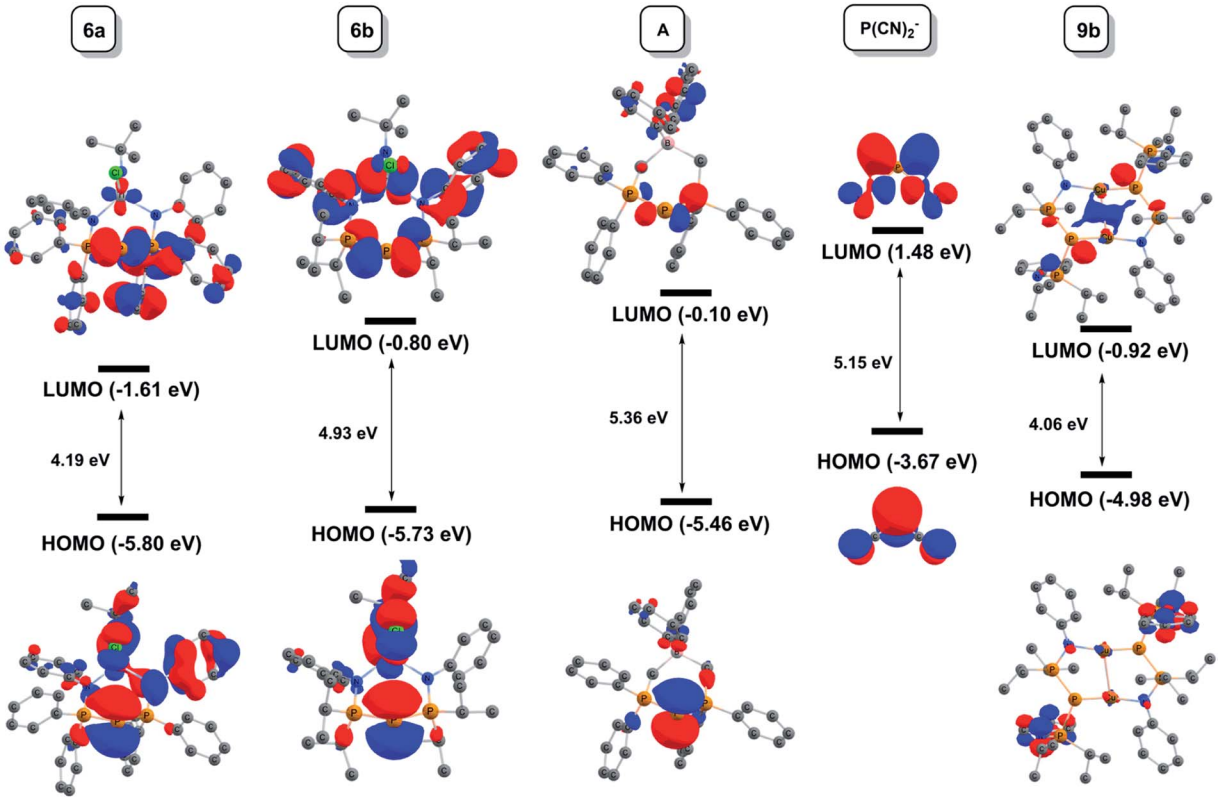

Fig. 4 HOMO and LUMO for complexes **6a**, **6b**, A, $P(CN)_2^-$ and **9b** (cut-off 0.05).

the antibonding interactions of this atom and its neighbours. Interestingly, the HOMO–LUMO gaps are comparable, which indicates that **BIPP** complexes could well be ambiphilic, just like other dicoordinate phosphorus compounds.** In this respect, it is worth noting the considerably lower LUMO energy of **6a** compared to **6b** ($\Delta E = -0.74$ eV), which suggests that the former should display enhanced electrophilicity. Additionally, the larger HOMO–LUMO gap of **6b** compared to **6a** is consistent with the more shielded signal of the central phosphorus atom in the $^{31}P\{^1H\}$ NMR spectrum ($\Delta\delta P_C = 61.8$ ppm).[65]

Electrostatic Potential Maps (EPM). In order to visualize charge distribution, we plotted the electrostatic potential map (EPM) for each computed compound.[94] The central phosphorus atom of **BIPP** compounds and **A** appears to be negatively charged, whilst lateral phosphorus atoms are positively charged (Fig. 5). This is consistent with the AIM results (see the ESI†). In **6a** and **6b** the negative charge distribution on the central phosphorus points towards the positively charged titanium atom, thus evidencing the electrostatic nature of the P–Ti interaction (*vide infra*).

Coordination of AuCl (**7b**) visibly reduces the maximum charge on the central phosphorus atom, although AIM calculations show that the net (negative) charge actually increases upon going from **6b** ($Q(P_C) = -0.15$) to **7b** ($Q(P_C) = -0.29$).

Topological analysis of bonding (ELF and AIM). Molecular orbitals provide valuable information about the energy and symmetry of electronic levels which can be useful, *e.g.* to predict reactivity. However, the trade-off in terms of explanatory power

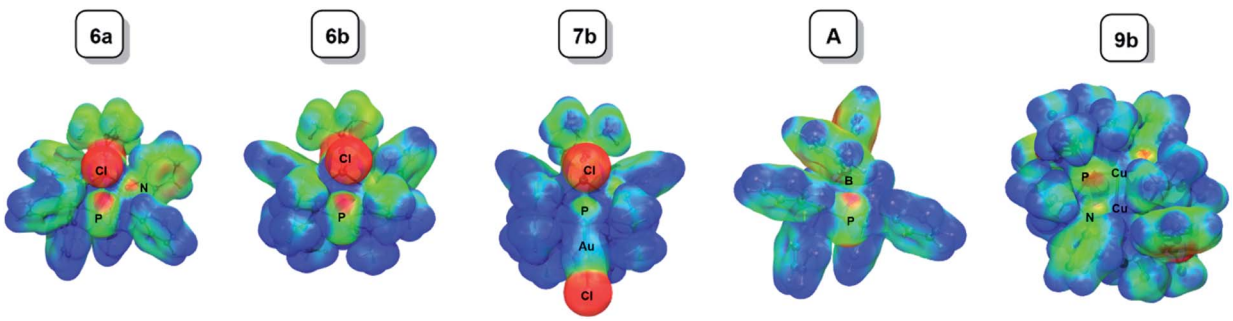

Fig. 5 Electrostatic potential maps for **6a**, **6b**, **7b**, A and **9b** plotted over the range −0.05 a.u. (red) to 0.05 a.u. (blue). The isosurfaces are drawn at 0.01 e $a.u.^{-3}$.

is a delocalized view of electrons in molecules that is at variance with the chemically intuitive notion of localized bonds and lone pairs inherited from Lewis. In order to reconcile a localized view of electrons with quantum mechanics, several methods and theories have been developed, such as the Electron Localization Function (ELF),[89] or the Quantum Theory of Atoms in Molecules (QTAIM).[96]

The ELF is a mathematical function that relates to the probability of finding an electron pair in the vicinity of a particular point in space. It is scaled so that $0 \leq \mathrm{ELF} \leq 1$ and increases with the increasing probability of finding a localized electron pair. The topological analysis of the ELF leads to a partition into several "basins" that can be mapped to chemical concepts: core electrons, bonds and lone pairs. In this paper, we have chosen to plot so-called *f*-localization domains, which are regions of space where ELF > *f*. Fig. 6 displays the *f*-localization domains ($f = 0.8$) of **6a**, **6b**, **7b**, **9b**, **A** and $\mathbf{P(CN)_2^-}$ separated into lone pair and valence basins.

Looking at the lone pair basins depicted in Fig. 6, the similarity between neutral **BIPP** complexes **6a–6b**, zwitterionic **TP** compound **A** and anionic $\mathbf{P(CN)_2^-}$ is evident: indeed, these compounds all possess two lone pairs of electrons at the central phosphorus atom. Coordination of AuCl to this phosphorus atom (**7b**) logically leaves one available lone pair, as noted elsewhere.[34–36,67]

Looking at the cylindrically shaped valence basins related to the P–P bonds, the similarity is again evident in the case of **6a–6b** and **A**, which lends further credence to the view of **BIPP** as **TP**

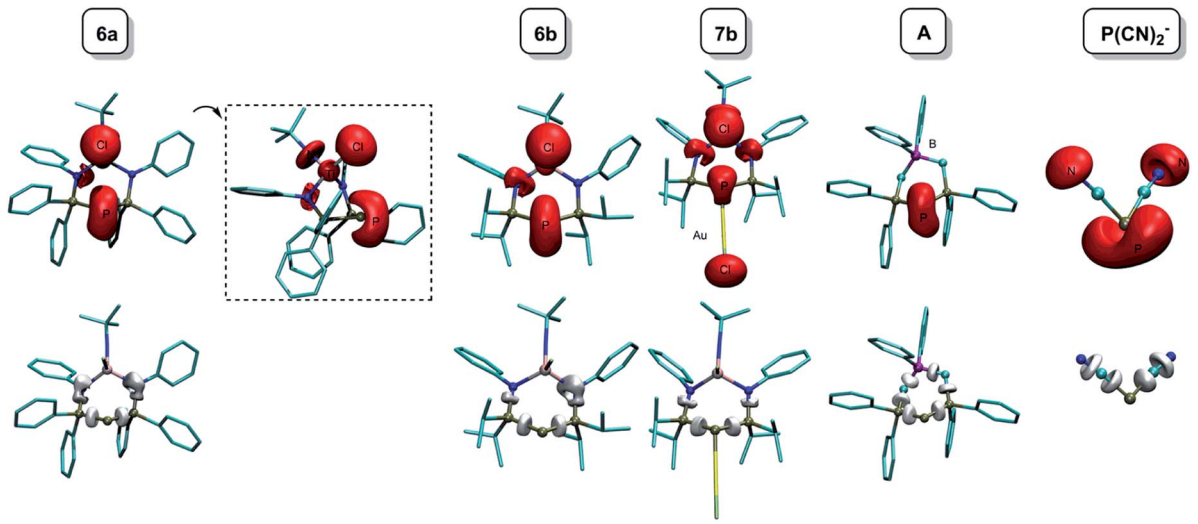

Fig. 6 Graphical representation of the ELF localization domains ($f = 0.8$) for **6a**, **6b**, **7b**, **A** and $\mathbf{P(CN)_2^-}$. Top: lone pair basins; bottom: valence basins.

Table 3 Relevant AIM topological indexes

	BCP	ρ (e Å^{-3})	$\nabla^2\rho$ (e Å^{-5})	G/ρ (E_h e^{-1})	H/ρ (E_h e^{-1})	DI
6a	P–P	0.857	−4.531	0.287	−0.658	1.022
	P–P	0.844	−4.386	0.278	−0.642	1.011
	P–Ti	0.115	0.940	0.647	−0.071	0.085
6b	P–P	0.844	−4.362	0.263	−0.626	1.042
	P–P	0.837	−4.241	0.262	−0.617	1.033
A	P–P	0.837	−4.265	0.286	−0.644	1.027
	P–P	0.857	−4.579	0.298	−0.670	1.044
$\mathbf{P(CN)_2^-}$	P–C	0.992	6.266	1.259	−0.816	1.023
7b	P–P	0.776	−3.061	0.290	−0.564	0.869
	P–P	0.776	−3.012	0.290	−0.562	0.876
	P–Ti	0.135	1.060	0.627	−0.070	0.099
9b	P–P	0.817	−3.928	0.238	−0.574	0.986
	P–P	0.769	−3.350	0.215	−0.519	0.910

compounds with anionic substituents. The situation is different in the case of $\mathbf{P(CN)_2}^-$: the valence basins associated with the P–C bonds are visibly deformed and point towards the central phosphorus atom, suggesting the presence of polarized (or dative) bonds. The presence of AuCl in **7b** also modifies the electron distribution associated with the P–P bonds, *i.e.* the valence basins point towards the AuCl moiety.

The QTAIM is a topological analysis of the properties of the electron density (ρ), its gradient ($\nabla\rho$) and its Laplacian ($\nabla^2\rho$) in the three-dimensional Euclidean space. Within the framework of the QTAIM, atoms emerge as non-overlapping regions of space (atomic basins) defined by their kinetic energies, and separated by interatomic surfaces.[96,100] Generally, bonded atoms are connected by a bond path (BP) crossing a bond critical point (BCP), *i.e.* a saddle point of the electron density.[101]

The numerical values of a series of topological indexes at BCPs enable to characterize the type of bonds between atoms: these are the delocalization index (DI, the number of delocalized electron pairs between two atoms), H/ρ and G/ρ ratios (where H is the total energy density, and G the kinetic energy density), in addition to ρ and $\nabla^2\rho$.†† Taken together, these parameters can help differentiate *open-shell* (normal covalent), *intermediate* (polar and/or dative covalent) and *closed-shell* (ionic, van der Waals) interactions. Of particular interest for our purposes is the DI, which has been shown to be a reliable measure of bond order;[102] thus, normal covalent bonds typically display DI values close to the formal bond order (~1 in the case of a single bond), whilst dative covalent bonds yield lower values (<1), and closed-shell interactions give DI values close to 0.[22,103]

We performed AIM calculations for complexes **6a**, **6b**, **7b** and **9b**, along with **A** and $\mathbf{P(CN)_2}^-$. For the sake of conciseness, only the P–P bonds (P–C for $\mathbf{P(CN)_2}^-$) and the P–Ti interaction are presented in Table 3.[104]

P–P bonds. The principal outcome of these calculations is that P–P bonds in **BIPP** complexes and the model **TP** compound **A** are best described as normal covalent bonds. Indeed, in every computed molecule the P–P BCPs display low (*i.e.* <1) G/ρ and negative H/ρ ratios, along with DI values close to unity; these results unambiguously indicate a normal covalent bond between light atoms, rather than a donor–acceptor interaction.[103] On the other hand, the moderate ρ (~0.84 e Å^{-3}) and $|\nabla^2\rho|$ (~4.0 e Å^{-5}) suggest relatively low bond dissociation energies (BDEs), as observed experimentally in the case of **A**.[34]

In order to investigate the nature of the P–P interaction in **6a** and **6b** in more details, we plotted the contour plot of $\nabla^2\rho$ in the P–P–P plane and the graph of $\nabla^2\rho$ along the P–P BPs (Fig. 7). The charge concentration due to the normal covalent interaction between the lateral and central phosphorus atoms is clearly visible in the contour plot (top).

Upon closer inspection of the Laplacian along the P–P bond path (bottom), additional features become apparent. Firstly, the BCP lies close to a local minimum (a characteristic of normal covalent bonds), and it is located in a rather flat region of the Laplacian; therefore, the P–P interaction cannot be described as a donor–acceptor bond, since this type of bonds entails much higher charge concentration in the atomic basin of the donor (*i.e.* the Laplacian profile should be much steeper). However, the BCP also lies ~0.3 Å closer to the more electropositive central phosphorus. The slight polarisation of the P–P bond towards the lateral phosphorus atom is actually quite remarkable, given the large charge difference between both atoms (*e.g.* for **6a**: $Q(P_L) = 2.11$ and 2.13; $Q(P_C) = -0.06$; see the ESI† for the full table). Overall, the best Lewis representation of **BIPP** complexes is the alternating dipolar form (see **BIPM**, Scheme 3, center), and our results suggest that this is also the case for **TP** compounds.

Different results were obtained for the $\mathbf{P(CN)_2}^-$ anion; in this case, the P–C bond is characterized by a positive value of $\nabla^2\rho$ at the BCP, a high kinetic energy ($G/\rho > 1$), a negative total energy ($H/\rho \ll 0$) and a DI close to unity. Moreover, the BCP lies closer to the more electropositive phosphorus atom. This picture is consistent either with a heteropolar covalent bond, or to a donor–acceptor interaction with considerable back-bonding, *e.g.* as in ($[Co(CO)_4]_2$).[103] Therefore, although dicoordinate phosphorus compounds such as **A** and $\mathbf{P(CN)_2}^-$ readily undergo heterolytic P–P and P–C bond cleavage in solution, the indiscriminate use of the term "ligand exchange" to qualify these reactions could be deceptive in view of the contrasting bonding situations.

P–Ti interaction. The AIM calculations also gave insights into the nature of the P_C–Ti interaction in **BIPP** complexes. According to the computed topological indexes at the **BCP**, the P–Ti

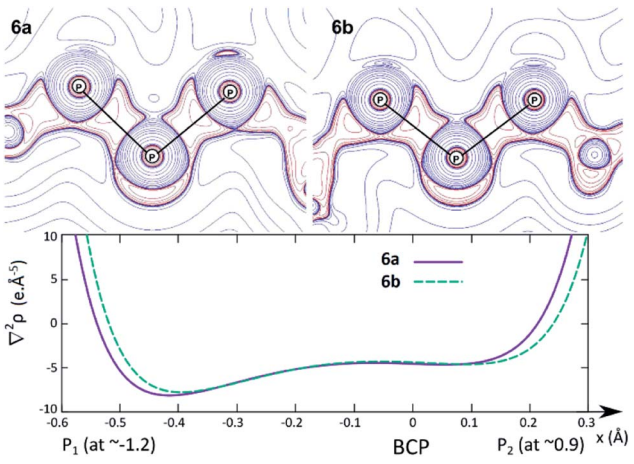

Fig. 7 Top: contour map of $\nabla^2\rho$ in the P–P–P plane for **6a** and **6b** (red lines indicate charge concentration and blue lines indicate charge depletion). Bottom: graph of $\nabla^2\rho$ along the left-hand P–P BPs for **6a** and **6b**.

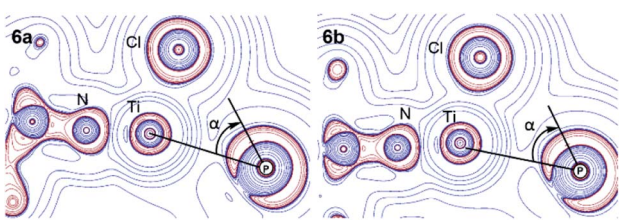

Fig. 8 Contour map of $\nabla^2\rho$ in the P_C–Ti–Cl plane for **6a** and **6b** (red lines indicate charge concentration and blue lines indicate charge depletion).

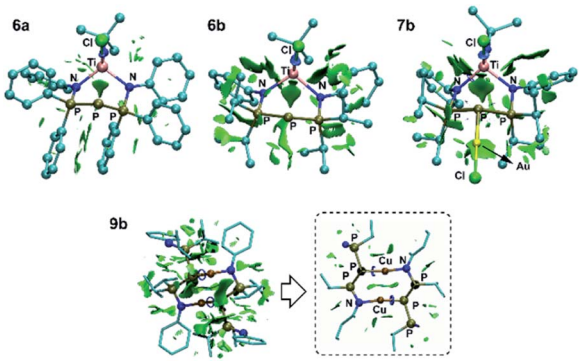

Fig. 9 NCI plot for **6a**, **6b**, **7b** and **9b**. Gradient isosurface ($s = 0.3$ a.u.) are colored according to a blue-green-red scheme over the range of $-8.00 < \text{sign}(\lambda 2)(\rho < 8.00$ a.u.). Green indicates very weak interaction.

interaction in **6a** can be described as weakly electrostatic, as witnessed by the very low electron density ($\rho = 0.115$ e Å^{-3}), the positive Laplacian ($\nabla^2\rho = 0.940$ e Å^{-5}), and the low value of the delocalization index (DI = 0.085). Also, the contour plot of the Laplacian in the P_C–Ti–Cl plane shows that the valence shell charge concentration (VSCC) corresponding to the lone pair of P pointing towards Ti is not aligned with the P–Ti BP (Fig. 8). This misalignment—evidenced by the angle α—is strongly reminiscent of the situation observed by Mitzel in a family of aminosilanes exhibiting weak intramolecular N–Si interactions.[105–108]

Interestingly, the values of G/ρ and H/ρ for the P–Ti interaction are at variance with the correspondence rules established by Macchi and Sironi,[103,109] in particular the negative total energy density (H) is surprising given the closed-shell nature of the interaction. This is probably due to a small admixture of covalent character, and highlights the fact that correspondence rules between topological indexes and chemical concepts should be taken with the proverbial pinch of salt, especially in the case of unusual bonding situations.

It should also be noted that a BCP was not found between P_C and Ti in the case of **6b**; however, the similar aspects of the contour plots shown in Fig. 8 suggest that the absence of a BCP is probably due to a "catastrophe point" in the molecular graph of **6b** (*i.e.* the BCP disappears after a threshold P–Ti distance).[110] The fact that a BCP "reappears" upon coordination of AuCl (complex **7b**) is consistent with this hypothesis. Essentially, the P–Ti interaction is similar in **6a** and **6b**.

Non-covalent interactions (NCI). The topological analysis of bonding situations was completed (for **6a**, **6b**, **7b** and **9b**) by non-covalent interactions maps obtained by plotting regions of space with both low density (ρ) and low reduced density gradient (s).[98,99] We found that P–Ti and Cu–Cu interactions are indeed non-covalent, in line with the AIM results (Fig. 9).

Conclusions

Although the first **BIPP** derivative was reported some 35 years ago by Schmidpeter, and despite the obvious analogy with P(IV)-stabilized methanediides (*e.g.* **BIPM**), the coordination chemistry of **BIPP** was an unexplored area before we undertook the present study. This apparent anomaly is undoubtedly related to their challenging synthesis, which requires the use of white phosphorus in order to install the central P atom. In the presence of early transition metals, **BIPP** act as peculiar *fac*-coordinating ligands: the soft central phosphorus atom mainly interacts electrostatically with the early metal, leaving enough electron density to bind late transition metals (such as Cu or Au). In the absence of an early metal, they switch to a κ^2-P,N coordination mode in order to bind Cu more strongly. Interestingly they do not seem to share **BIPM**'s propensity to engage in multiple bonding interactions with transition metals. These intriguing coordination properties certainly warrant further studies, *e.g.* with *f*-group elements and late transition metals.

The key feature of **BIPP** is their similarity to triphosphenium cations (**TP**): indeed, as evidenced computationally, **BIPP**s may be regarded as **TP** bearing anionic substituents, and hence as *ambiphilic phosphides*. An important practical consequence is that they should undergo heterolytic P–P bond cleavage under relatively mild conditions. Crucially, the topological analysis of the computed electron density and its Laplacian demonstrate that the P–P bonds in these compounds are normal covalent: we therefore suggest reconsidering the terminology currently employed to describe their reactivity (*i.e.* nucleophilic substitution *vs.* ligand exchange). Our results also indicate that homolytic bond cleavage might be observed under suitable conditions (*e.g.* in nonpolar solvents).

Finally, a word of caution is in order: experimentally, **TP** behave like labile main group donor–acceptor adducts. Hence, the use of the arrow formalism will inevitably mislead some authors into thinking that the P–P bonds are dative covalent. To be sure, the arrow formalism is merely a heuristic device, but the key point is that it is not used consistently by chemists: it can take different meanings depending on one's perspective on chemical bonds and their representations. In the end, it does not really matter which representation is used, as long as chemists take precautions in order to avoid misinterpretations of their drawings.

Experimental section

Synthesis

Carefully read the risk assessment and cautionary notes in the ESI† before carrying out any procedure involving white phosphorus.

White phosphorus (P_4). In an Ar glovebox, red phosphorus (12.4 g, 0.400 mol) was placed in a fused silica glass Schlenk tube (general electric, semiconductor grade) greased with Apiezon H grease. The vessel was removed from the glovebox and evacuated at a vacuum line for 5 min. The vessel was positioned almost horizontally with a very slight twist, in order to force the flow of liquid P_4 towards the stopper (see picture in the ESI,† step 1). A 2000 W heat gun at full power was placed underneath the pile of red phosphorus and moved progressively (*ca.* 30 min) towards the bottom end of the vessel. After cooling, the vessel was taken into the glovebox and scraped with a spatula. The gathered solids were extracted during the night with 500 mL of CH_2Cl_2 in a normal borosilicate Schlenk flask. The suspension was filtered over a grade 4 sintered glass frit, the

red solid was dried on the frit; this residue (5.7 g) can be reused to make white phosphorus, although ideally it should be mixed with fresh red phosphorus. The solution was evaporated to dryness, and finely divided P_4 was obtained and stored away from light in the glovebox freezer (4.5 g, yield 83%).

2a. In an Ar glovebox, lithium phosphinoamide **1a** (4.29 g, 12.0 mmol) and white phosphorus (2.97 g, 24.0 mmol) were suspended in 1,4-dioxane (30 mL) in a Schlenk flask. The vessel was transferred into a sand bath at 100 °C, stirred for a couple of minutes under Ar, then closed under slight static vacuum (quick 180° rotation of the stopcock). The heterogeneous reaction mixture quickly turned dark brown and was heated to 100 °C for 66 h, after which it was allowed to cool to room temperature, and filtered over a sintered glass frit in the glovebox. The black cake was rinsed with 1,4-dioxane, and the filtrate was evaporated to dryness outside of the glovebox. Upon returning to the glovebox, the solid residue was triturated in 50 mL of pentane and stirred until a fine powder was obtained. The powder was filtered over a sintered glass frit and rinsed with pentane (4 × 10 mL), then dried on the frit. Compound **2a** was obtained as a pale yellow powder (3.20 g, yield 81%). Elemental analysis: calculated for $C_{40}H_{38}LiN_2O_2P_3$: C 70.80, H 5.64, N 4.13; found: C 70.53, H 5.47, N 4.06.

2b. In an Ar glovebox, lithium phosphinoamide **1b** (1.78 g, 8.3 mmol) and white phosphorus (2.06 g, 16.6 mmol) were suspended in 1,4-dioxane (20 mL) in a Schlenk flask. A vivid pink color was observed immediately. The vessel was transferred into a sand bath at 100 °C, stirred for a couple of minutes under Ar, then closed under slight static vacuum (quick 180° rotation of the stopcock). The heterogeneous reaction mixture quickly turned dark brown and was heated to 100 °C for 13 h, after which it was allowed to cool to room temperature, and filtered over a sintered glass frit in the glovebox. The black cake was rinsed with pentane, and the filtrate was evaporated to dryness outside of the glovebox. Upon returning to the glovebox, the solid residue was dissolved in 15 mL of pentane stored in the glovebox freezer at −20 °C. Yellow crystals **2b** were collected and dried on a frit (0.65 g, yield 31%). Elemental analysis: calculated for $C_{28}H_{46}LiN_2O_2P_3$: C, 61.99; H, 8.55; N, 5.16. Found: C, 62.13; H, 9.22; N, 5.29.

2b′. In an Ar glovebox, lithium phosphinoamide **1b** (4.00 g, 18.2 mmol) and white phosphorus (1.13 g, 9.10 mmol) were suspended in THF (70 mL) in a Schlenk flask. A vivid pink color was observed immediately. The vessel was transferred into an oil bath at 65 °C, stirred for a couple of minutes under Ar, then closed under slight static vacuum (quick 180° rotation of the stopcock). The heterogeneous reaction mixture quickly turned dark brown and was heated to 65 °C for 40 min, after which it was allowed to cool to room temperature, and another portion of P_4 (1.13 g, 9.10 mmol) was added. The mixture was heated again for 45 min and this procedure was repeated twice, (overall amount of P_4: 4.50 g, 36.3 mmol). Analysis of the reaction mixture revealed that the reaction was not complete, therefore it was heated again at 65 °C for 2 h. After cooling, the mixture was filtered over a sintered glass frit in the glovebox. The black cake was rinsed with pentane, and the filtrate was evaporated to dryness outside of the glovebox. Upon returning to the glovebox, the solid residue was dissolved in 100 mL of pentane and evaporated again. Addition of 30 mL of pentane followed by agitation then storage in the glovebox freezer at −20 °C for two days afforded orange crystals. The crystals were collected, crushed and dried on a frit, yielding **2b′** as an orange powder (1.25 g, yield 26%). Single crystals suitable for X-ray diffraction analysis were grown by cooling a saturated solution of **2b′** in pentane at −20 °C. Elemental analysis: calculated for $C_{28}H_{46}LiN_2OP_3$: C, 63.87; H, 8.81; N, 5.32. Found: C, 63.15; H, 9.00; N, 5.34.

3a. In an Ar glovebox, proligand **2a** (2.63 g, 3.86 mmol) and $[TiCl_3(THF)_3]$ (1.48 g, 4.00 mmol) were suspended in THF (20 mL). The reaction mixture was stirred for 14 h, during which a pale green precipitate appeared. The suspension was filtered over a sintered glass frit (porosity grade 4), the solid was rinsed with THF (3 × 10 mL) and dried on the frit, yielding **3a** as a blue-green powder (2.28 g, yield 74%). Single crystals suitable for X-ray diffraction were grown by cooling a saturated THF solution of **3a** at −20 °C. Elemental analysis: calculated for $C_{40}H_{38}Cl_2N_2OP_3Ti$: C, 62.04; H, 4.95; N, 3.62. Found: C, 61.69; H, 5.15; N, 3.61.

3b. In an Ar glovebox, ligand **2b** (0.537 g, 1.20 mmol) and $[TiCl_3(THF)_3]$ (0.371 g, 1.20 mmol) were suspended in THF (5 mL). The reaction mixture turned quickly into a clear emerald green solution. After stirring overnight, a bright yellow precipitate appeared. The suspension was filtered over a sintered glass frit (porosity grade 4), the solid was rinsed with cold THF (2 × 1.5 mL) and dried on the frit, yielding **3b** as a bright yellow powder (0.367 g, yield 52%). Single crystals suitable for X-ray diffraction were grown by cooling a saturated THF solution of **3b** at −20 °C. Elemental analysis: calculated for $C_{24}H_{38}Cl_2N_2P_3Ti$: C, 50.91; H, 6.76; N, 4.95. Found: C, 50.65; H, 6.82; N, 4.85.

4a. In an Ar glovebox, complex **3a** (194 mg, 0.250 mmol) and $[Cp_2Fe][BPh_4]$ (126 mg, 0.250 mmol) were mixed in THF (3 mL). The reaction mixture turned quickly red. Sodium 3,5-dimethylphenolate etherate was added and the mixture was stirred for 5 min. The resulting solution was evaporated to dryness and the residue was triturated in toluene to remove ferrocene. The residue was dissolved in 3 mL of CH_2Cl_2, filtered over a plug of diatomaceous earth, and an orange solid was precipitated by addition to 50 mL of pentane under vigorous agitation. The solid was filtered over a sintered glass frit, suspended and washed with toluene (3 × 5 mL), then pentane (3 × 5 mL). After drying on the frit under vacuum for 20 min, complex **4a** was obtained as an orange powder containing 50 mol% of CH_2Cl_2 and 15 mol% of pentane (202 mg, yield 66%). Single crystals suitable for X-ray diffraction were obtained by diffusion of pentane into a CH_2Cl_2 solution of **4a** at −20 °C. Elemental analysis: a satisfactory elemental analysis could not be obtained; carbon was always too low. This problem has been encountered previously with BPh_4^- salts of Ti, see ref. 64.

5a. In an Ar glovebox, zirconium tetrachloride (233 mg, 1.00 mmol) and proligand **2a** (679 mg, 1.00 mmol) were suspended in toluene. The reaction mixture was stirred for 14 h, then filtered on a sintered glass frit and the resulting solid was rinsed with toluene (3 × 3 mL). The solid was suspended in 10 mL of CH_2Cl_2, filtered over a pad of diatomaceous earth, and the

filtrate was evaporated to dryness. The residue was triturated in 5 mL of pentane, filtered on a sintered glass frit and dried on the frit, yielding **5a** as a white powder containing 50 mol% of CH_2Cl_2 (550 mg, yield 67%). Single crystals suitable for X-ray diffraction were grown by slow diffusion of pentane into a CH_2Cl_2 solution of **5a** at −20 °C. Elemental analysis: calculated for $C_{36}H_{30}Cl_3N_2P_3Zr(CH_2Cl_2)_{0.5}$: C, 53.23; H, 3.79; N, 3.40. Found: C, 54.63; H, 4.18; N, 3.46.

5b. In an Ar glovebox, zirconium tetrachloride (233 mg, 1.0 mmol) and proligand **2b** (602 mg, 1.0 mmol) were suspended in dry toluene. The reaction mixture was stirred overnight, then filtered on a sintered glass frit and the resulting solid was rinsed with toluene (3 × 3 mL). The solid was suspended in 10 mL of CH_2Cl_2, filtered over a pad of diatomaceous earth, and the filtrate was evaporated to dryness. The residue was triturated in 5 mL of pentane, filtered on a sintered glass frit, rinsed with 2 × 5 mL of pentane and dried on the frit, yielding **5a** as a white powder (461 mg, yield 67%). Single crystals suitable for X-ray diffraction were grown by slow diffusion of pentane into a CH_2Cl_2 solution of **5b** at −20 °C. Elemental analysis: calculated for $C_{24}H_{38}Cl_3N_2P_3Zr$: C, 44.69; H, 5.94; N, 4.34. Found: C, 44.50; H, 5.93; N, 4.37.

6a-Py. In an Ar glovebox, $[TiCl_2(N^tBu)(Py)_3]$ (1.28 g, 3.00 mmol) and proligand **2a** (2.06 g, 3.00 mmol) were suspended in toluene (50 mL). The reaction mixture was stirred for 2 h 30, during which it turned gradually yellow. It was filtered over a sintered glass frit, and the resulting solid was dissolved in CH_2Cl_2 and filtered over a pad of diatomaceous earth. The filtrate was evaporated to dryness outside of the glovebox. Upon returning to the glovebox, the resulting solid was stirred in 20 mL of pentane overnight. The suspension was filtered over a sintered glass frit, and the resulting solid was suspended in 5 mL of pentane and filtered, then dried on the frit. Complex **6a-Py** was obtained as a yellow powder (1.21 g, yield 50%). Single crystals suitable for X-ray diffraction were grown by slow diffusion of pentane into a CH_2Cl_2 solution of **6a-Py** at −20 °C. Elemental analysis: calculated for $C_{45}H_{44}ClN_4P_3Ti$: C, 66.15; H, 5.43; N, 6.86. Found: C, 66.35; H, 5.49; N, 6.71.

6a. In an Ar glovebox, complex **6a-Py** (0.37 g, 0.45 mmol) was suspended in toluene (40 mL) in a Schlenk flask. Outside of the box, the vessel was connected to a Schlenk line and the reaction mixture was heated until a light reflux was observed. An oil bubbler was used to prevent any build-up of pressure during heating. The solid dissolved gradually, and the solution became paler. The oil bubbler war closed and the reaction mixture was allowed to cool to room temperature. Pentane (100 mL) was added to precipitate a microcrystalline solid, which was filtered on a sintered glass frit in the glovebox. The solid was dried under vacuum at a Schlenk line, yielding **6a** as a pale yellow powder containing 100 mol% of toluene (320 mg, yield 74%). Single crystals suitable for X-ray diffraction were obtained by slow diffusion of pentane into a CH_2Cl_2 solution of **6a** at −20 °C. Elemental analysis: calculated for $C_{40}H_{39}ClN_3P_3Ti(C_8H_8)$: C, 68.00; H, 5.71; N, 5.06. Found: C, 67.78; H, 6.10; N, 5.02.

6b. In an Ar glovebox, $[TiCl_2(N^tBu)(Py)_3]$ (620 mg, 1.45 mmol) and proligand **2b** (827 mg, 1.52 mmol) were suspended in toluene (50 mL). The reaction mixture was filtered over a pad of diatomaceous earth. The filtrate was evaporated to dryness outside of the glovebox. Upon returning to the glovebox, the resulting solid was stirred in 30 mL of pentane for 5 min. The suspension was filtered over a sintered glass frit, and the resulting solid was suspended three times in pentane (5 mL) and filtered, then dried on the frit. Complex **6b** was obtained as a pale yellow powder (705 mg, yield 81%). Single crystals suitable for X-ray diffraction were grown by slow diffusion of pentane into a CH_2Cl_2 solution of **6b** at −20 °C. Elemental analysis: calculated for $C_{28}H_{47}ClN_3P_3Ti$: C, 55.87; H, 7.87; N, 6.98. Found: C, 55.86; H, 8.44; N, 7.25.

7b. In an Ar glovebox, [Au(THT)Cl] (240 mg, 0.750 mmol) and complex **6b** (451 mg, 0.750 mmol) were suspended in CH_2Cl_2 and the reaction mixture was stirred for 5 min, then evaporated to dryness outside of the glovebox. Upon returning to the glovebox, the resulting solid was stirred in 10 mL of pentane for 15 min. The suspension was filtered over a sintered glass frit, and the resulting solid was suspended in 5 mL of pentane and filtered, then dried on the frit. Analysis of the solid by ^{1}H NMR spectroscopy revealed the presence of residual THT, pentane and CH_2Cl_2. The solid was heated under vacuum in a warm bath (40 °C) for 1 h, thus drastically reducing the content of pentane and CH_2Cl_2, but not THT. The solid was stirred in 5 mL of pentane for 1 h, filtered over a sintered glass frit and dried on the frit, affording complex **7b** was obtained as a white powder (300 mg, yield 48%). The moderate yield is essentially due to the solubility of **7b** in pentane, since it is the only observable product by ^{1}H and ^{31}P NMR spectroscopy when the reaction is performed *in situ* on an analytical scale. Single crystals suitable for X-ray diffraction were grown by slow diffusion of pentane into a CH_2Cl_2 solution of **7b** at −20 °C. Complex **7b** slowly degrades in solutions of CD_2Cl_2 or C_6D_6 at room temperature, but can be stored for several months in the solid state at −20 °C under argon without significant degradation. Elemental analysis: calculated for $C_{28}H_{47}AuCl_2N_3P_3Ti$: C, 40.31; H, 5.68; N, 5.04. Found: C, 40.21; H, 5.60; N, 4.86.

8b. In an Ar glovebox, [CuBr] (36 mg, 0.25 mmol) and complex **6b** (151 mg, 0.250 mmol) were suspended in CH_2Cl_2 and the reaction mixture was stirred for 10 min, during which it turned orange-brown. A small amount of white solid was removed by filtration over a pad of diatomaceous earth. The reaction mixture was then evaporated to dryness outside of the glovebox. Upon returning to the glovebox, the resulting solid was stirred in 10 mL of pentane, and the suspension was filtered over a sintered glass frit. The resulting solid was suspended three times in pentane (5 mL) and filtered, then dried on the frit. Complex **8b** was obtained as a light brown powder containing 50 mol% of pentane (152 mg, yield 78%). Single crystals suitable for X-ray diffraction were grown by slow diffusion of pentane into a CH_2Cl_2 solution of **8b** at −20 °C. Elemental analysis: calculated for $C_{28}H_{47}BrClCuN_3P_3Ti(C_5H_{12})_{0.5}$: C, 46.88; H, 6.84; N, 5.38. Found: C, 46.60; H, 7.30; N, 5.39.

9b. In an Ar glovebox, proligand **2b** (200 mg, 0.33 mmol) and [CuBr] (48 mg, 0.33 mmol) were suspended in toluene (25 mL). The resulting beige slurry was stirred at room temperature for 5 days. Volatiles were removed under vacuum outside of the

glovebox. The resulting beige solid was suspended in 20 mL of CH_2Cl_2 and the suspension was filtered over a pad of diatomaceous earth. The filtrate was evaporated to dryness. The solid residue was stirred in 20 mL of pentane overnight. Upon returning in the glovebox, the yellow slurry was filtered over a sintered glass frit and dried under vacuum, yielding complex **9b** as a white powder containing 80 mol% of pentane (121 mg, yield 67%). Single crystals suitable for X-ray diffraction were obtained by slow diffusion of pentane into a CH_2Cl_2 solution of **9b** at −20 °C. Elemental analysis: calculated for $C_{48}H_{76}Cu_2N_4P_6(C_5H_{12})_{0.8}$: C, 57.84; H, 7.99; N, 5.19. Found: C, 57.42; H, 8.13; N, 4.95.

Attempted syntheses and failed experiments

See the ESI.†

Computational details

All calculations were performed using the Gaussian 16 package,[111] and the B3PW91 hybrid functional on the real experimental systems.[112] Gold and copper atoms were described with the LANL2DZ pseudopotential.[113] The 6-31+G(d,p) basis set were employed for all other atoms. This basis set will be denoted as BS1. Optimizations were carried out without any symmetry restrictions taking into solvent effect (toluene) by means of the continuum standard solvation PCM model.[114] All stationary points computed were fully optimized. All total energies and Gibbs free energies have been zero-point energy (ZPE) and temperature corrected using unscaled density functional frequencies. Molecular orbitals were plotted using ChemCraft.[115]

In order to gain insight into the nature of the chemical bonding, we performed atoms in molecules analysis (QTAIM),[95,96] using AIMALL software,[116] and Electronic Localized Function analysis using TopChem package.[117] The Electrostatic Potential Surface (EPS) map and NCIPLOT[98,99] have been plotted with VMD software.[118] For AIM, ELF and NCI analyses, wavefunction was recomputed using RIFIT basis sets for gold and Cu atoms (NCI only for Cu) and 6-31+G(d,p) for all other atoms using geometries obtained at the PCM (Toluene)-B3PW91-D3/BS1 level.

The B3PW91/BS1 level was also used for the time-dependant DFT computations. We tested that using the larger def2-TZVP basis set did not change the computed wavelengths.[119]

Conflicts of interest

There are no conflicts to declare.

Acknowledgements

We are indebted to Dr Nicolas Mézailles for sharing his vast knowledge of white phosphorus with us. We thank T. A. Keith for his help in plotting the Laplacian along a bond critical path. The authors also thank the "Plateforme d'Analyse Chimique et de Synthèse Moléculaire de l'Université de Bourgogne" (PACSMUB, http://www.wpcm.fr) for access to spectroscopy and instrumentation, Mr Marcel Soustelle (University of Burgundy, ICMUB, PACSMUB) for elemental analyses and Prof Ewen Bodio (University of Burgundy, ICMUB, OCS team) for access to SAFAS Flx-Xenius XC spectrofluorimeter. Financial support from Centre National de la Recherche Scientifique (CNRS), Université de Bourgogne (UB), Agence Nationale de la Recherche (ALCATRAS, ANR-16-CE07-0001-01), Conseil Regional de Bourgogne (PARI CDEA program), Conseil Régional de Bourgogne Franche-Comté (PhosFerTiMn project), Fonds Européen de Développement Régional (FEDER) and the PIA-excellence ISITE-BFC program (COMICS project) is gratefully acknowledged. Calculations were performed using HPC resources from DSI-CCUB (Université de Bourgogne).

Notes and references

§ Incidentally, the usage of the arrow to "fix the octet" has recently been appraised theoretically, and it turns out that for some molecules (*e.g.* H_2SO_4, HNO_3 or $HClO_4$),[120,121] the dissociation of oxygen is actually heterolytic; thus, for these molecules, the arrow formalism also corresponds to Haaland's definition. We thank an anonymous reviewer for opening our eyes to the different usages of the arrow formalism, and to the fact that according to Sidgwick, the D → A and D^+–A^- representations are strictly equivalent.

¶ The term "divalent" instead of "dicoordinate" is often encountered in the literature. However, as pointed by a reviewer, the latter is less ambiguous since it does not presuppose the number of electrons involved in bonding. For a rigorous discussion on valence and coordination number, see ref. 122.

‖ We did not react **2b** with [AuCl(THT)], however **2b** and **2b′** can be used indifferently, for example to synthesize **3b** or **6b**.

** Due to the negative charge, the HOMO and LUMO energies of $\mathbf{P(CN)_2^-}$ are considerably higher than those of **BIPP** and **TP** compounds; we computed the molecular orbitals of $[P(CN)_2][K]$ and found that the energies were lowered by 2.48 eV (LUMO) and 1.66 eV (HOMO). Hence the HOMO–LUMO gap of $[P(CN)_2][K]$ is comparable to those of **6a** and **6b**.

†† The ellipticity (ε) is also commonly used to assess bond multiplicity, however we have found that the obtained values are sometimes meaningless (*e.g.* for the P–Ti interaction).

1 T. Cantat, N. Mezailles, A. Auffrant and P. Le Floch, *Dalton Trans.*, 2008, 1957–1972.
2 T. K. Panda and P. W. Roesky, *Chem. Soc. Rev.*, 2009, **38**, 2782–2804.
3 S. T. Liddle, D. P. Mills and A. J. Wooles, *Chem. Soc. Rev.*, 2011, **40**, 2164–2176.
4 S. Harder, *Coord. Chem. Rev.*, 2011, **255**, 1252–1267.
5 M. Fustier-Boutignon, N. Nebra and N. Mézailles, *Chem. Rev.*, 2019, **119**, 8555–8700.
6 R. Tonner, F. Öxler, B. Neumüller, W. Petz and G. Frenking, *Angew. Chem., Int. Ed.*, 2006, **45**, 8038–8042.
7 R. Tonner and G. Frenking, *Chem.–Eur. J.*, 2008, **14**, 3260–3272.
8 L. Zhao, M. Hermann, N. Holzmann and G. Frenking, *Coord. Chem. Rev.*, 2017, **344**, 163–204.
9 C. A. Dyker and G. Bertrand, *Nat. Chem.*, 2009, **1**, 265–266.
10 M. Alcarazo, C. W. Lehmann, A. Anoop, W. Thiel and A. Fürstner, *Nat. Chem.*, 2009, **1**, 295–301.
11 L. Zhao, S. Pan, N. Holzmann, P. Schwerdtfeger and G. Frenking, *Chem. Rev.*, 2019, **119**, 8781–8845.
12 H. Schmidbaur, *Angew. Chem., Int. Ed.*, 2007, **46**, 2984–2985.

13 G. Frenking, B. Neumüller, W. Petz, R. Tonner and F. Öxler, *Angew. Chem., Int. Ed.*, 2007, **46**, 2986–2987.
14 H. Daniel, K. Ingo and S. Andreas, *Angew. Chem., Int. Ed.*, 2014, **53**, 6047–6048.
15 G. Frenking, *Angew. Chem., Int. Ed.*, 2014, **53**, 6040–6046.
16 D. Himmel, I. Krossing and A. Schnepf, *Angew. Chem., Int. Ed.*, 2014, **53**, 370–374.
17 Ligand exchange reactions have been observed in a P,S-double ylides and in a Si(0) silylene, see (*a*) N. Dellus, T. Kato, N. Saffon-Merceron, V. Branchadell and A. Baceiredo, *Inorg. Chem.*, 2011, **50**, 7949–7951; (*b*) K. C. Mondal, H. W. Roesky, M. C. Schwarzer, G. Frenking, I. Tkach, H. Wolf, D. Kratzert, R. Herbst-Irmer, B. Niepötter and D. Stalke, *Angew. Chem., Int. Ed.*, 2013, **52**, 1801–1805.
18 A. Haaland, *Angew. Chem., Int. Ed.*, 1989, **28**, 992–1007.
19 N. V. Sidgwick, *The Theory of Electronic Valency*, Oxford University Press, London, 1929.
20 V. I. Minkin, *Pure Appl. Chem.*, 1999, **71**, 1919.
21 I. Abdellah, C. Lepetit, Y. Canac, C. Duhayon and R. Chauvin, *Chem.–Eur. J.*, 2010, **16**, 13095–13108.
22 N. A. Pushkarevsky, P. A. Petrov, D. S. Grigoriev, A. I. Smolentsev, L. M. Lee, F. Kleemiss, G. E. Salnikov, S. N. Konchenko, I. Vargas-Baca, S. Grabowsky, J. Beckmann and A. V. Zibarev, *Chem.–Eur. J.*, 2017, **23**, 10987–10991.
23 S. Mebs and J. Beckmann, *J. Phys. Chem. A*, 2017, **121**, 7717–7725.
24 A. Nandi and S. Kozuch, *Chem.–Eur. J.*, 2020, **26**, 759–772.
25 A. Schmidpeter, *Heteroat. Chem.*, 1999, **10**, 529–537.
26 P. K. Coffer and K. B. Dillon, *Coord. Chem. Rev.*, 2013, **257**, 910–923.
27 B. D. Ellis and C. L. B. Macdonald, *Coord. Chem. Rev.*, 2007, **251**, 936–973.
28 E. M. Dionisi, J. F. Binder, J. H. W. LaFortune and C. L. B. Macdonald, *Dalton Trans.*, 2020, **49**, 12115–12127.
29 S. Lochschmidt and A. Schmidpeter, *Z. Naturforsch., B: Anorg. Chem., Org. Chem.*, 1985, **40**, 765–773.
30 A. Schmidpeter, S. Lochschmidt and W. S. Sheldrick, *Angew. Chem., Int. Ed.*, 1985, **24**, 226–227.
31 S. C. Kosnik, G. J. Farrar, E. L. Norton, B. F. T. Cooper, B. D. Ellis and C. L. B. Macdonald, *Inorg. Chem.*, 2014, **53**, 13061–13069.
32 J. F. Binder, A. a. Swidan, M. Tang, J. H. Nguyen and C. L. B. Macdonald, *Chem. Commun.*, 2015, **51**, 7741–7744.
33 S. C. Kosnik and C. L. B. Macdonald, *Dalton Trans.*, 2016, **45**, 6251–6258.
34 J. W. Dube, C. L. B. Macdonald and P. J. Ragogna, *Angew. Chem., Int. Ed.*, 2012, **51**, 13026–13030.
35 S. C. Kosnik, M. C. Nascimento, J. F. Binder and C. L. B. Macdonald, *Dalton Trans.*, 2017, **46**, 17080–17092.
36 J. F. Binder, S. C. Kosnik and C. L. B. Macdonald, *Chem.–Eur. J.*, 2018, **24**, 3556–3565.
37 J. F. Binder, A. a. Swidan and C. L. B. Macdonald, *Inorg. Chem.*, 2018, **57**, 11717–11725.
38 J. Zhou, L. L. Liu, L. L. Cao and D. W. Stephan, *Angew. Chem., Int. Ed.*, 2019, **58**, 18276–18280.
39 For other "ligand exchange" reactions at phosphorus, see (*a*) N. Burford, T. S. Cameron, P. J. Ragogna, E. Ocando-Mavarez, M. Gee, R. McDonald and R. E. Wasylishen, *J. Am. Chem. Soc.*, 2001, **123**, 7947–7948; (*b*) N. Burford, P. J. Ragogna, R. McDonald and M. J. Ferguson, *J. Am. Chem. Soc.*, 2003, **125**, 14404–14410; (*c*) M. M. Hansmann, R. Jazzar and G. Bertrand, *J. Am. Chem. Soc.*, 2016, **138**, 8356–8359; (*d*) M. M. Hansmann and G. Bertrand, *J. Am. Chem. Soc.*, 2016, **138**, 15885–15888; (*e*) M. Donath, E. Conrad, P. Jerabek, G. Frenking, R. Fröhlich, N. Burford and J. J. Weigand, *Angew. Chem., Int. Ed.*, 2012, **51**, 2964–2967.
40 IUPAC, *Compendium of Chemical Terminology (the "Gold Book")*, compiled by A. D. McNaught and A. Wilkinson, Blackwell Scientific Publications, Oxford, 2nd edn, 1997, online version (2019) created by S. J. Chalk. ISBN 0-9678550-9-8, DOI: 10.1351/goldbook.
41 B. D. Ellis and C. L. B. Macdonald, *Inorg. Chem.*, 2006, **45**, 6864–6874.
42 A. Kasani, R. P. Kamalesh Babu, R. McDonald and R. G. Cavell, *Angew. Chem., Int. Ed.*, 1999, **38**, 1483–1484.
43 R. G. Cavell, R. P. Kamalesh Babu, A. Kasani and R. McDonald, *J. Am. Chem. Soc.*, 1999, **121**, 5805–5806.
44 C. M. Ong and D. W. Stephan, *J. Am. Chem. Soc.*, 1999, **121**, 2939–2940.
45 T. Cantat, T. Arliguie, A. Noël, P. Thuéry, M. Ephritikhine, P. L. Floch and N. Mézailles, *J. Am. Chem. Soc.*, 2009, **131**, 963–972.
46 J.-C. Tourneux, J.-C. Berthet, P. Thuery, N. Mezailles, P. Le Floch and M. Ephritikhine, *Dalton Trans.*, 2010, **39**, 2494–2496.
47 J.-C. Tourneux, J.-C. Berthet, T. Cantat, P. Thuéry, N. Mézailles and M. Ephritikhine, *J. Am. Chem. Soc.*, 2011, **133**, 6162–6165.
48 J.-C. Tourneux, J.-C. Berthet, T. Cantat, P. Thuéry, N. Mézailles, P. Le Floch and M. Ephritikhine, *Organometallics*, 2011, **30**, 2957–2971.
49 G. Ma, M. J. Ferguson, R. McDonald and R. G. Cavell, *Inorg. Chem.*, 2011, **50**, 6500–6508.
50 W. Ren, X. Deng, G. Zi and D.-C. Fang, *Dalton Trans.*, 2011, **40**, 9662–9664.
51 O. J. Cooper, D. P. Mills, J. McMaster, F. Moro, E. S. Davies, W. Lewis, A. J. Blake and S. T. Liddle, *Angew. Chem., Int. Ed.*, 2011, **50**, 2383–2386.
52 D. P. Mills, O. J. Cooper, F. Tuna, E. J. L. McInnes, E. S. Davies, J. McMaster, F. Moro, W. Lewis, A. J. Blake and S. T. Liddle, *J. Am. Chem. Soc.*, 2012, **134**, 10047–10054.
53 V. H. Gessner, F. Meier, D. Uhrich and M. Kaupp, *Chem.–Eur. J.*, 2013, **19**, 16729–16739.
54 O. J. Cooper, D. P. Mills, J. McMaster, F. Tuna, E. J. L. McInnes, W. Lewis, A. J. Blake and S. T. Liddle, *Chem.–Eur. J.*, 2013, **19**, 7071–7083.
55 M. Gregson, E. Lu, J. McMaster, W. Lewis, A. J. Blake and S. T. Liddle, *Angew. Chem., Int. Ed.*, 2013, **52**, 13016–13019.
56 M. Gregson, E. Lu, F. Tuna, E. J. L. McInnes, C. Hennig, A. C. Scheinost, J. McMaster, W. Lewis, A. J. Blake, A. Kerridge and S. T. Liddle, *Chem. Sci.*, 2016, **7**, 3286–3297.

57 E. Lu, S. Sajjad, V. E. J. Berryman, A. J. Wooles, N. Kaltsoyannis and S. T. Liddle, *Nat. Commun.*, 2019, **10**, 634.
58 A recent study by Gessner and Frenking suggests that this is due to the increased electron-sharing character of the P–C bonds conferred by the phosphinoamide substituents: L. T. Scharf, D. M. Andrada, G. Frenking and V. H. Gessner, *Chem.–Eur. J.*, 2017, **23**, 4422–4434.
59 A. Schmidpeter and G. Burget, *Angew. Chem., Int. Ed.*, 1985, **24**, 580–581.
60 A. Schmidpeter and G. Bürget, *Z. Naturforsch., B: Anorg. Chem., Org. Chem.*, 1985, **40**, 1306.
61 A. T. Normand, C. G. Daniliuc, B. Wibbeling, G. Kehr, P. Le Gendre and G. Erker, *J. Am. Chem. Soc.*, 2015, **137**, 10796–10808.
62 A. T. Normand, C. G. Daniliuc, G. Kehr, P. Le Gendre and G. Erker, *Dalton Trans.*, 2016, **45**, 3711–3714.
63 A. T. Normand, C. G. Daniliuc, B. Wibbeling, G. Kehr, P. Le Gendre and G. Erker, *Chem.–Eur. J.*, 2016, **22**, 4285–4293.
64 A. T. Normand, Q. Bonnin, S. Brandès, P. Richard, P. Fleurat-Lessard, C. H. Devillers, C. Balan, P. Le Gendre, G. Kehr and G. Erker, *Chem.–Eur. J.*, 2019, **25**, 2803–2815.
65 J. W. Dube, C. L. B. Macdonald, B. D. Ellis and P. J. Ragogna, *Inorg. Chem.*, 2013, **52**, 11438–11449.
66 P. K. Coffer, R. M. K. Deng, K. B. Dillon, M. A. Fox and R. J. Olivey, *Inorg. Chem.*, 2012, **51**, 9799–9808.
67 K. Schwedtmann, M. H. Holthausen, K.-O. Feldmann and J. J. Weigand, *Angew. Chem., Int. Ed.*, 2013, **52**, 14204–14208.
68 J. W. Dube, V. A. Béland, P. D. Boyle and P. J. Ragogna, *Can. J. Chem.*, 2015, **93**, 253–264.
69 Macdonald reported an alternative method for the synthesis of $[PPh_4][P(CN)_2]$ during the course of our study: J. F. Binder, S. C. Kosnik, P. B. J. St Onge and C. L. B. Macdonald, *Chem.–Eur. J.*, 2018, **24**, 14644–14648.
70 H. B. Baker, *Philos. Trans. R. Soc., A*, 1888, **179**, 571–591.
71 C. W. Hsu, Y. C. Tsai, B. M. Cossairt, C. Camp, J. Arnold, B. M. Cossairt, B. M. Cossairt, C. C. Cummins and Y. C. Tsai, *Inorg. Synth.*, 2019, 123–134.
72 B. Cordero, V. Gomez, A. E. Platero-Prats, M. Reves, J. Echeverria, E. Cremades, F. Barragan and S. Alvarez, *Dalton Trans.*, 2008, 2832–2838.
73 S. Alvarez, *Dalton Trans.*, 2013, **42**, 8617–8636.
74 This is in contrast with phosphidotitanocene compounds in which superhyperfine coupling to P was observed, see ref. 64.
75 A. T. Normand, P. Richard, C. Balan, C. G. Daniliuc, G. Kehr, G. Erker and P. Le Gendre, *Organometallics*, 2015, **34**, 2000–2011.
76 Methanediide complexes have been shown to display metal–ligand cooperativity (FLP-type behavior), see (*a*) R. P. Kamalesh Babu, R. McDonald and R. G. Cavell, *Organometallics*, 2000, **19**, 3462–3465; (*b*) K.-S. Feichtner and V. H. Gessner, *Chem. Commun.*, 2018, **54**, 6540–6553.
77 B. J. Coe and S. J. Glenwright, *Coord. Chem. Rev.*, 2000, **203**, 5–80.
78 A. T. Normand, A. Massard, P. Richard, C. Canovas, C. Balan, M. Picquet, A. Auffrant and P. Le Gendre, *Dalton Trans.*, 2014, **43**, 15098–15110.
79 A. Glöckner, T. Bannenberg, S. Büschel, C. G. Daniliuc, P. G. Jones and M. Tamm, *Chem.–Eur. J.*, 2011, **17**, 6118–6128.
80 F. Lindenberg, T. Shribman, J. Sieler, E. Hey-Hawkins and M. S. Eisen, *J. Organomet. Chem.*, 1996, **515**, 19–25.
81 R. T. Baker, W. C. Fultz, T. B. Marder and I. D. Williams, *Organometallics*, 1990, **9**, 2357–2367.
82 F. Dielmann, E. V. Peresypkina, B. Krämer, F. Hastreiter, B. P. Johnson, M. Zabel, C. Heindl and M. Scheer, *Angew. Chem., Int. Ed.*, 2016, **55**, 14833–14837.
83 B. P. Johnson, F. Dielmann, G. Balázs, M. Sierka and M. Scheer, *Angew. Chem., Int. Ed.*, 2006, **45**, 2473–2475.
84 K. Angermaier, E. Zeller and H. Schmidbaur, *J. Organomet. Chem.*, 1994, **472**, 371–376.
85 G. A. Bowmaker, S. E. Boyd, J. V. Hanna, R. D. Hart, P. C. Healy, B. W. Skelton and A. H. White, *J. Chem. Soc., Dalton Trans.*, 2002, 2722–2730.
86 C.-M. Che, Z. Mao, V. M. Miskowski, M.-C. Tse, C.-K. Chan, K.-K. Cheung, D. L. Phillips and K.-H. Leung, *Angew. Chem., Int. Ed.*, 2000, **39**, 4084–4088.
87 W.-F. Fu, X. Gan, C.-M. Che, Q.-Y. Cao, Z.-Y. Zhou and N. N.-Y. Zhu, *Chem.–Eur. J.*, 2004, **10**, 2228–2236.
88 M. Nishikawa, T. Sano, M. Washimi, K. Takao and T. Tsubomura, *Dalton Trans.*, 2016, **45**, 12127–12136.
89 A. D. Becke and K. E. Edgecombe, *J. Chem. Phys.*, 1990, **92**, 5397–5403.
90 B. Silvi and A. Savin, *Nature*, 1994, **371**, 683–686.
91 P. Fuentealba, E. Chamorro and J. C. Santos, in *Theoretical and Computational Chemistry*, ed. A. Toro-Labbé, Elsevier, 2007, vol. 19, pp. 57–85.
92 M. Causá, A. Savin and B. Silvi, *Found. Chem.*, 2014, **16**, 3–26.
93 Y. Grin, A. Shavin and B. Silvi, in *The Chemical Bond*, ed. G. Frenking and S. Shaik, 2014, vol. 1, pp. 345–382.
94 T. Clark, in *The Chemical Bond*, ed. G. Frenking and S. Shaik, 2014, vol. 2, pp. 523–536.
95 R. F. W. Bader, *Chem. Rev.*, 1991, **91**, 893–928.
96 R. Bader, *Atoms in molecules: a quantum theory*, Oxford University Press, 1994.
97 P. Lode and A. Popelier, in *The Chemical Bond*, ed. G. Frenking and S. Shaik, 2014, vol. 1, pp. 271–308.
98 E. R. Johnson, S. Keinan, P. Mori-Sánchez, J. Contreras-García, A. J. Cohen and W. Yang, *J. Am. Chem. Soc.*, 2010, **132**, 6498–6506.
99 J. Contreras-García, E. R. Johnson, S. Keinan, R. Chaudret, J.-P. Piquemal, D. N. Beratan and W. Yang, *J. Chem. Theory Comput.*, 2011, **7**, 625–632.
100 R. F. W. Bader, *J. Phys. Chem. A*, 2010, **114**, 7431–7444.
101 However it should be emphasized that there is no strict equivalence between BCPs and chemical bonds, see (*a*) R. F. W. Bader, *J. Phys. Chem. A*, 2009, **113**, 10391–10396; (*b*) C. Foroutan-Nejad, S. Shahbazian and R. Marek, *Chem.–Eur. J.*, 2014, **20**, 10140–10152; (*c*) Z. A. Keyvani, S. Shahbazian and M. Zahedi, *Chem.–Eur. J.*, 2016, **22**, 5003–5009; (*d*) S. Shahbazian, *Chem.–Eur. J.*, 2018, **24**, 5401–5405.

102 C. Outeiral, M. A. Vincent, Á. Martín Pendás and P. L. A. Popelier, *Chem. Sci.*, 2018, **9**, 5517–5529.
103 P. Macchi and A. Sironi, *Coord. Chem. Rev.*, 2003, **238–239**, 383–412.
104 For a detailed analysis of the P–Au, P–Cu and Cu–Cu interactions in **7b** and **9b**, see the ESI.† Our conclusions regarding the polar single bond nature of the P/N interaction in **BIPP** compounds (which should therefore be written P^{+}–N^{-}, not P═N) are similar to those formulated by Stalke: N. Kocher, D. Leusser, A. Murso and D. Stalke, *Chem.–Eur. J.*, 2004, **10**, 3622–3631.
105 N. W. Mitzel, U. Losehand, A. Wu, D. Cremer and D. W. H. Rankin, *J. Am. Chem. Soc.*, 2000, **122**, 4471–4482.
106 N. W. Mitzel, K. Vojinović, T. Foerster, H. E. Robertson, K. B. Borisenko and D. W. H. Rankin, *Chem.–Eur. J.*, 2005, **11**, 5114–5125.
107 N. W. Mitzel, K. Vojinović, R. Fröhlich, T. Foerster, H. E. Robertson, K. B. Borisenko and D. W. H. Rankin, *J. Am. Chem. Soc.*, 2005, **127**, 13705–13713.
108 M. Hagemann, R. J. F. Berger, S. A. Hayes, H.-G. Stammler and N. W. Mitzel, *Chem.–Eur. J.*, 2008, **14**, 11027–11038.
109 P. Macchi, D. M. Proserpio and A. Sironi, *J. Am. Chem. Soc.*, 1998, **120**, 13429–13435.
110 Obviously, the computed distance for **6b** is superior to that threshold, but we note that the experimental solid state value is lower by 6–7 % (Table 2). We do not think that this is due to a failure of the computations to reproduce the P–Ti bond distance accurately. Rather, this difference probably originates from the different permittivities (ε) of toluene and the bulk crystal. For enlightening studies of medium effects on chemical bonds, see ref. 105–108 and: (*a*) H. Jiao and P. v. R. Schleyer, *J. Am. Chem. Soc.*, 1994, **116**, 7429–7430; (*b*) K. R. Leopold, M. Canagaratna and J. A. Phillips, *Acc. Chem. Res.*, 1997, **30**, 57–64. For detailed discussions on the "chemical meaning" of molecular graphs and BCPs, see ref. 101.
111 M. J. Frisch, G. W. Trucks, H. B. Schlegel, G. E. Scuseria, M. A. Robb, J. R. Cheeseman, G. Scalmani, V. Barone, G. A. Petersson, H. Nakatsuji, X. Li, M. Caricato, A. V. Marenich, J. Bloino, B. G. Janesko, R. Gomperts, B. Mennucci, H. P. Hratchian, J. V. Ortiz, A. F. Izmaylov, J. L. Sonnenberg, D. Williams-Young, F. Ding, F. Lipparini, F. Egidi, J. Goings, B. Peng, A. Petrone, T. Henderson, D. Ranasinghe, V. G. Zakrzewski, J. Gao, N. Rega, G. Zheng, W. Liang, M. Hada, M. Ehara, K. Toyota, R. Fukuda, J. Hasegawa, M. Ishida, T. Nakajima, Y. Honda, O. Kitao, H. Nakai, T. Vreven, K. Throssell, J. A. Montgomery Jr, J. E. Peralta, F. Ogliaro, M. J. Bearpark, J. J. Heyd, E. N. Brothers, K. N. Kudin, V. N. Staroverov, T. A. Keith, R. Kobayashi, J. Normand, K. Raghavachari, A. P. Rendell, J. C. Burant, S. S. Iyengar, J. Tomasi, M. Cossi, J. M. Millam, M. Klene, C. Adamo, R. Cammi, J. W. Ochterski, R. L. Martin, K. Morokuma, O. Farkas, J. B. Foresman and D. J. Fox, *Gaussian 16, Revision B.01*, Gaussian, Inc., Wallingford CT, 2016.
112 (*a*) A. D. Becke, *J. Chem. Phys.*, 1993, **98**, 5648–5652; (*b*) J. P. Perdew, in *Electronic Structure of Solids*, ed. P. Ziesche and H. Eschrig, Akademie-Verlag, Berlin, 1991, p. 11.
113 P. J. Hay and W. R. Wadt, *J. Chem. Phys.*, 1985, **82**, 299–310.
114 J. Tomasi, B. Mennucci and R. Cammi, *Chem. Rev.*, 2005, **105**, 2999–3094.
115 *ChemCraft – graphical software for visualization of quantum chemistry computations*, https://www.chemcraftprog.com, last visited June, 3rd 2020.
116 T.-A. Keith, *AIMAll (version 17.11.14B), TK Gristmill Software*, Overland Park KS, USA, 2014.
117 D. Kozlowski and J. Pilmé, *J. Comput. Chem.*, 2011, **32**, 3207–3217.
118 (*a*) W. Humphrey, A. Dalke and K. Schulten, *J. Mol. Graphics*, 1996, **14**, 33–38; (*b*) http://www.ks.uiuc.edu/Research/vmd/.
119 F. Weigend and R. Ahlrichs, *Phys. Chem. Chem. Phys.*, 2005, **7**, 3297–3305.
120 A. Kalemos and A. Mavridis, *J. Phys. Chem. A*, 2009, **113**, 13972–13975.
121 B. A. Jackson, J. Harshman and E. Miliordos, *J. Chem. Educ.*, 2020, **97**, 3638–3646.
122 G. Parkin, *J. Chem. Educ.*, 2006, **83**, 791.